Lithuanian Journal of Physics
Vol. **66**, No. 3, pp. 164–184 (2026)
ISSN 1648-8504 eISSN 2424-3647
DOI: https://doi.org/10.3952/physics.2026.66.3.4

SECOND-ORDER RAYLEIGH–SCHRÖDINGER PERTURBATION THEORY FOR THE GRASP2018 PACKAGE: THREE-PARTICLE FEYNMAN DIAGRAM CONTRIBUTION TO CORE–VALENCE CORRELATIONS

G. Gaigalas, P. Rynkun, and L. Kitovienė

Institute of Theoretical Physics and Astronomy, Faculty of Physics, Vilnius University, Saulėtekio 3, 10257 Vilnius, Lithuania
Email: gediminas.gaigalas@tfai.vu.lt; pavel.rynkun@tfai.vu.lt; laima.radziute@tfai.vu.lt

Received 3 February 2026; accepted 14 May 2026

In order to ascertain the precise atomic characteristics, it is important to incorporate a wide range of electron correlations in the computational analysis. However, it is important to note that undertaking such studies will result in substantial increases of the configuration state function expansions. The present publication, as well as the series of articles that have been published by G. Gaigalas, P. Rynkun, and L. Kitovienė, are dedicated to the analysis and resolution of the problem in question. In this series, a method was developed based on second-order perturbation theory to identify the most important core–valence, core, core–core, and valence–valence correlations. The method under discussion is based on a combination of the relativistic configuration interaction method and the stationary second-order Rayleigh–Schrödinger many-body perturbation theory in an irreducible tensorial form. In this study, the method is further expanded to encompass additional core–valence electron correlations of the third and fourth types. Conversely, the correlations that are not encompassed by perturbation theory are addressed in a conventional manner. This method can be used to calculate the properties of an atom or ion with any number of valence and core electrons. As an example of its application, the atomic calculations of the energy structure and lifetime for Ne II are presented.

Keywords: configuration interaction, spin-angular integration, perturbation theory, tensorial algebra, valence–valence correlations, core–valence correlations, core correlations, core–core correlations

1. Introduction

In this work, a further development of the second-order Rayleigh–Schrödinger many-body perturbation theory (RSMBPT) [1] in an irreducible tensorial form [2–6] is presented for a computational package GRASP [7, 8] based on the multiconfiguration Dirac–Hartree–Fock (MCDHF) approximation and the relativistic configuration interaction (RCI) method [9–11]. This combination greatly facilitates the selection of the configuration state function (CSF) space in a way that does not sacrifice computational accuracy but minimizes the space itself in the RCI method.

In this paper, the methodology is extended to core–valence correlations, which are conditioned by a three-particle Feynman diagram. Although in this case a large number of CSFs that represent these correlations do not enter the computation, for completeness of the methodology and for developing a general algorithm, we consider this extension to be important in the generation of the CSF space [12]. Moreover, this extension facilitates the use of the methodology for complex systems.

Similarly, as in our previous papers [2–6], we have provided in this paper (Section 2) the analytical expression of a three-particle Feynman diagram describing the core–valence correlations with explanations. Since the spin-angular part of this diagram is much more complex, a significant part of the paper is devoted to calculating

the spin-angular coefficients [13, 14] and the extension of library `librang` [15] (Section 3). The final expressions are presented in Section 4 of the paper. Section 5 contains the calculations showing that the expressions and the examination of the core–valence correlations presented in the paper are correct and usable. Conclusions are presented in Section 6.

2. Relativistic second-order effective Hamiltonian of an atom or ion in an irreducible tensorial form for the remaining core–valence correlations

New Feynman diagrams are used to describe core–valence (CV) correlations, which were not available for core (C) [3], core–core (CC) [4], and valence–valence (VV) [5] correlations. We discuss this in detail below.

2.1. The third type of core–valence correlations

The first two types of core–valence correlations are already described in the paper [2]. The third type of core–valence correlations is presented through the Feynman diagram CV_7 from Fig. 1, where all lines with the double arrow of diagram are renamed in the following way: $p' \equiv m$ and $m' = n = n' = p \equiv n$.

$$(n_a\ell_a)\, j_a^{\,2j_a+1}\, (n_m\ell_m)\, j_m^{w_m}\, (n_n\ell_n)\, j_n^{w_n} \rightarrow$$
$$\rightarrow (n_a\ell_a)\, j_a^{2j_a}\, (n_m\ell_m)\, j_m^{w_m-1}\, (n_n\ell_n)\, j_n^{w_n+2}. \qquad (1)$$

The three-particle Feynman diagram's CV_7 expression, like the diagrams described in the previous papers [2–6], have an energy denominator $D = \sum (\varepsilon_{\mathrm{down}} - \varepsilon_{\mathrm{up}})$, where $\varepsilon_{\mathrm{down}}$ ($\varepsilon_{\mathrm{up}}$) is the single-particle eigenvalue associated with the down- (up-) orbital lines to (from) the lowest interaction line of the diagram. For example, the denominators for the CV_7 diagram are

$$D = (\varepsilon_a + \varepsilon_{p'} - \varepsilon_n - \varepsilon_p), \qquad (2)$$

where the index a belongs to the F set, and p', n, p belong to the F' set of orbitals [2].

Also, the following notations are used in the expressions of this diagram (see Fig. 1):

$$X_k(ij, i'j') = \langle \ell_i j_i \| C^{(k)} \| \ell_{i'} j_{i'} \rangle \, \langle \ell_j j_j \| C^{(k)} \| \ell_{j'} j_{j'} \rangle \times$$
$$\times R^k(n_i j_i\, n_j j_j,\, n_{i'} j_{i'}\, n_{j'} j_{j'}), \qquad (3)$$

where $R^k(n_i j_i n_j j_j,\ n_{i'} j_{i'} n_{j'} j_{j'})$ is the radial integral of electrostatic interaction between electrons (Ref. [10], Eqs. (89) and (90)) and $\langle \ell_i j_i \| C^{(k)} \| \ell_{i'} j_{i'} \rangle$ is the reduced matrix element of the irreducible tensor operator $C^{(k)}$ in the jj–coupling.

This diagram has six operators of second quantization (three pairs of creation and annihilation operators) as was in the paper [6]. This complicates finding the values of the spin-angular coefficient of this diagram and therefore makes the original program library `librang` [15] from Grasp unusable in the most general case. But for this case the problem was already solved in the paper [6] and the program library `librang` [15] was appropriately extended.

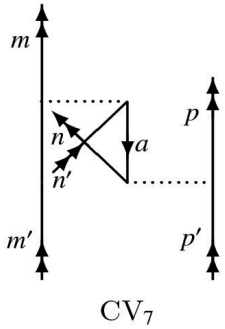

CV_7

$$= -\sum_{k,k',x} \sqrt{\frac{[x]}{[k,k']}} \sum_{m,m'} \sum_{n,n'} \sum_{p,p'}$$
$$\times \left[\left[\left[a^{(j_m)} \times \tilde{a}^{(j_{m'})} \right]^{(k)} \times \left[\tilde{a}^{(j_{n'})} \times a^{(j_n)} \right]^{(x)} \right]^{(k')} \times \left[a^{(j_p)} \times \tilde{a}^{(j_{p'})} \right]^{(k')} \right]^{(0)}$$
$$\times \sum_a \frac{1}{\left(\varepsilon_a + \varepsilon_{p'} - \varepsilon_n - \varepsilon_p\right)} \begin{Bmatrix} j_n & j_{n'} & x \\ k & k' & j_a \end{Bmatrix} X_k(ma, m'n')\; X_{k'}(np, ap')$$

Fig. 1. The CV Feynman diagram of the second-order effective Hamiltonian for the third and fourth types of core–valence correlations $(n_a\ell_a)\, j_a^{2j_a+1}\, (n_m\ell_m)\, j_m^{w_m}\, (n_n\ell_n)\, j_n^{w_n} \rightarrow (n_a\ell_a)\, j_a^{2j_a}\, (n_m\ell_m)\, j_m^{w_m-1}\, (n_n\ell_n)\, j_n^{w_n+2}$ and $(n_a\ell_a)\, j_a^{2j_a+1}\, (n_m\ell_m)\, j_m^{w_m}\, (n_n\ell_n)\, j_n^{w_n}\, (n_p\ell_p)\, j_p^{w_p} \rightarrow (n_a\ell_a)\, j_a^{2j_a}\, (n_m\ell_m)\, j_m^{w_m-1}\, (n_n\ell_n)\, j_n^{w_n+1}\, (n_p\ell_p)\, j_p^{w_p+1}$.

2.2. The fourth type of core–valence correlations

The following type of correlations

$$(n_a\ell_a)\, j_a^{2ja+1}\, (n_m\ell_m)\, j_m^{wm}\, (n_n\ell_n)\, j_n^{wn}\, (n_p\ell_p)\, j_p^{wp} \rightarrow$$

$$\rightarrow (n_a\ell_a)\, j_a^{2ja}\, (n_m\ell_m)\, j_m^{wm-1}\, (n_n\ell_n)\, j_n^{wn+1}\, (n_p\ell_p)\, j_p^{wp+1} \quad (4)$$

is described by the same diagram CV_7 with four different sets of open lines with double-arrow indices. Four diagrams A_1, A_2, A_3 and A_4 from Fig. 2 represent all these different sets. For example, the Feynman diagram A_1 has the following values: $m = p' \equiv m$, $m' = p \equiv n$ and $n = n' \equiv p$. Therefore, to find the value of this type of correlations, it is necessary to analyze all four diagrams: A_1, A_2, A_3 and A_4. But it is important to note that, to achieve the same result, the four diagrams can be easily replaced by just two diagrams, A_5 ($A_5 \equiv A_1$), A_6 ($A_6 \equiv A_3$), plus a multiplier (1 + P (...)), where the notation P ($n \rightleftharpoons p$) means that the indices n and p should be swapped. This makes it considerably easier to carry out the desired calculations. Note that A_5 describes the direct part of the correlation under consideration, while A_6 describes the exchange part of the interaction. These A_5 and A_6 are three-particle Feynman diagrams for which the program library `librang` [15] from Grasp does not support the calculation of spin-angular parts. It is therefore necessary to extend the capabilities of this program library to calculate the values of these diagrams. This problem will be discussed and solved in detail in the next section.

3. The spin-angular part of the three-particle Feynman diagram contributing to core– valence correlations

The program library `librang` [15] from Grasp evaluates spin-angular coefficients of any matrix element with any number of open subshells for any one- and/or two-particle operators. Therefore, in the

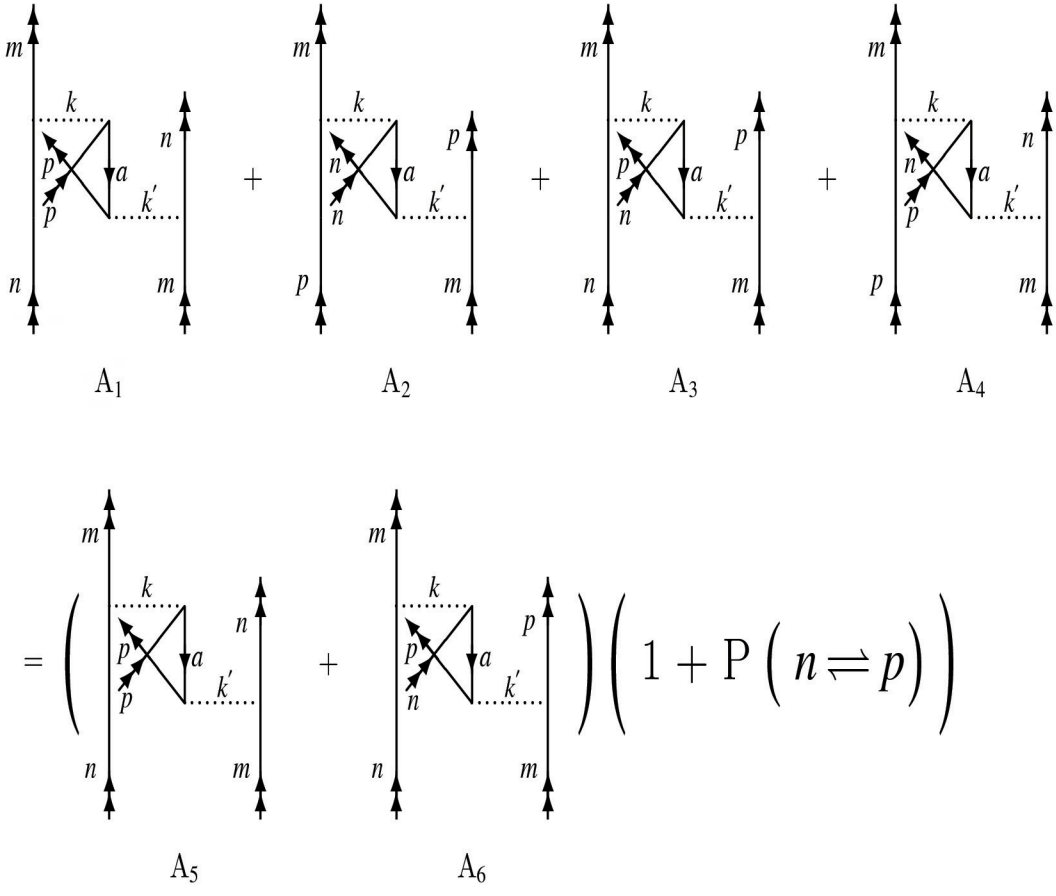

Fig. 2. The CV Feynman diagrams of the second-order effective Hamiltonian, expressing the fourth type of core–valence correlations $(n_a\ell_a)\, j_a^{2ja+1}\, (n_m\ell_m)\, j_m^{wm}\, (n_n\ell_n)\, j_n^{wn}\, (n_p\ell_p)\, j_p^{wp} \rightarrow (n_a\ell_a)\, j_a^{2ja}\, (n_m\ell_m)\, j_m^{wm-1}\, (n_n\ell_n)\, j_n^{wn+1}\, (n_p\ell_p)\, j_p^{wp+1}$.

previous papers [2–5], when developing the combination of second-order Rayleigh–Schrödinger perturbation theory and relativistic configuration interaction method, there was no problem in using it to find correlations described by vacuum, one- and two-particle Feynman diagrams. However, problems with using this library arise when dealing with three-particle operators [6].

The program library `librang` [15] is based on the spin-angular approach [13, 14, 16]. The specifics of this approach (factorization of standard values, interaction strengths, and recoupling matrices) make it easy enough to extend it to allow the program library to find the spin-angular part of the CV_7 Feynman diagram that is needed to find the correlations that are being studied in this paper. This can be done by using ideas published in the papers [17, 18], where the second quantization operators are grouped according to their action on the subshell, i.e. so that the second quantization operators acting on the subshell *m* first, then on the subshell *p* (if there are any), and finally on the subshell *n*. The spin-angular library extension, both in the paper [6] and in this paper, also uses quasispin symmetry and formalism [13, 14, 16], as in the original library `librang` [15]. This greatly facilitates spin-angular integration. Below, we show how this has been done for the different types of core–valence correlations separately described by a three-particle Feynman diagram.

3.1. The spin-angular part of the third type of core–valence correlations

In this case, the diagram CV_7 has the tensorial structure

$$\left[\left[\left[a_1^{(j_m)} \times \tilde{a}_2^{(j_n)}\right]^{(k)} \times \left[\tilde{a}_3^{(j_n)} \times a_4^{(j_n)}\right]^{(x)}\right]^{(k')} \times \right.$$
$$\left. \times \left[a_5^{(j_n)} \times \tilde{a}_6^{(j_m)}\right]^{(k')}\right]^{(0)}, \qquad (5)$$

where the subscript next to the operator indicates the sequence number of the second quantization operator in the tensorial product. As seen in the tensorial structure (5), two pairs of second quantization operators are mixed, i.e. they consist of the second quantization operators acting on different subshells. This is a pair consisting of operators with sequence numbers 1 and 2 and a pair with sequence numbers 5 and 6. This situation greatly complicates the study of the spin-angular part of this operator. But if we replace the tensorial structure (5) with the following

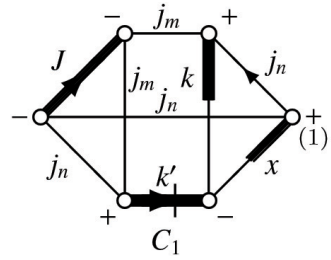

Fig. 3. Diagram showing the recoupling coefficient C_1.

$$\left[\left[a_1^{(j_m)} \times \tilde{a}_6^{(j_m)}\right]^{(J_1)} \times \left[\left[a_4^{(j_n)} \times \tilde{a}_3^{(j_n)}\right]^{(x)} \times \right.\right.$$
$$\left.\left. \times \left[\tilde{a}_2^{(j_n)} \times a_5^{(j_n)}\right]^{(J_2)}\right]^{(J_1)}\right]^{(0)}, \qquad (6)$$

then the situation would change and one could easily extend the spin-angular approach [13, 14, 16] to the study of three-particle operator for this type of correlations [18] as was done in the paper [6]. We also point out that this allows us to use all known symmetries of the atom, including the quasispin symmetry [13, 16], in the calculations.

There are several such options for the tensorial product. But we have chosen the form (6) because the transformation to (6) is similar to the transformation from Eq. (13) to (14) in the paper [6], and it is possible to make use of the recoupling coefficients of [6] represented by diagrams B_1 and B_2. But first of all, using the well-known commutation rule of secondary quantization (see, for example, Eq. (29) from Ref. [19], where expression is in the *LS*-coupling),

$$\left[\tilde{a}^{(j_i)} \times a^{(j_k)}\right]^{(x)} = -(-1)^{j_i+j_k-x}\left[a^{(j_k)} \times \tilde{a}^{(j_i)}\right]^{(x)} +$$
$$+\sqrt{[j_i]}\,\delta(n_i l_i j_i, n_k l_k j_k)\,\delta(x,0), \qquad (7)$$

we interchange the operators a_3 and a_4. This leads to the expression

$$\left[\left[\left[a_1^{(j_m)} \times \tilde{a}_2^{(j_n)}\right]^{(k)} \times \left[\tilde{a}_3^{(j_n)} \times a_4^{(j_n)}\right]^{(x)}\right]^{(k')} \times \right.$$
$$\left. \times \left[a_5^{(j_n)} \times \tilde{a}_6^{(j_m)}\right]^{(k')}\right]^{(0)} =$$
$$= (-1)^x \left[\left[\left[a_1^{(j_m)} \times \tilde{a}_2^{(j_n)}\right]^{(k)} \times \left[a_4^{(j_n)} \times \tilde{a}_3^{(j_n)}\right]^{(x)}\right]^{(k')} \times \right.$$
$$\left. \times \left[a_5^{(j_n)} \times \tilde{a}_6^{(j_m)}\right]^{(k')}\right]^{(0)} + \sqrt{[j_n]}\left[\left[a_1^{(j_m)} \times \tilde{a}_2^{(j_n)}\right]^{(k)} \times \right.$$
$$\left. \times \left[a_5^{(j_n)} \times \tilde{a}_6^{(j_m)}\right]^{(k')}\right]^{(0)} \delta(x,0)\delta(k,k'). \qquad (8)$$

Now, in the first part of expression (8), using the same commutation rule (7), after interchanging the operators of the first and third pair of the operators of secondary quantization, we get

$$\Big[\Big[[a_1^{(j_m)}\times\tilde{a}_2^{(j_n)}]^{(k)}\times[\tilde{a}_3^{(j_n)}\times a_4^{(j_n)}]^{(x)}\Big]^{(k')}\times$$
$$\times[a_5^{(j_n)}\times\tilde{a}_6^{(j_m)}]^{(k')}\Big]^{(0)}=$$
$$=(-1)^{x+k+k'}\Big[\Big[[\tilde{a}_2^{(j_n)}\times a_1^{(j_m)}]^{(k)}\times[a_4^{(j_n)}\times\tilde{a}_3^{(j_n)}]^{(x)}\Big]^{(k')}\times$$
$$\times[\tilde{a}_6^{(j_m)}\times a_5^{(j_n)}]^{(k')}\Big]^{(0)}+\sqrt{[j_n]}\Big[[a_1^{(j_m)}\times\tilde{a}_2^{(j_n)}]^{(k)}\times$$
$$\times[a_5^{(j_n)}\times\tilde{a}_6^{(j_m)}]^{(k')}\Big]^{(0)}\delta(x,0)\,\delta(k,k'). \tag{9}$$

Now, similarly to the case of the paper [6] (Eq. (7)), using the commutation rules of the operators of the second quantization and the graphical representation [20] of the angular momentum theory, we transform the first part of expression (9) into the tensorial structure (6), and the second part of the expression we transform in such a way that the pair of operators of the second quantization act on the same subshell. Thus, we get

$$\Big[\Big[[a_1^{(j_m)}\times\tilde{a}_2^{(j_n)}]^{(k)}\times[\tilde{a}_3^{(j_n)}\times a_4^{(j_n)}]^{(x)}\Big]^{(k')}\times$$
$$\times[a_5^{(j_n)}\times\tilde{a}_6^{(j_m)}]^{(k')}\Big]^{(0)}=(-1)^{x+k+k'}\,C_1\Big[[a_1^{(j_m)}\times\tilde{a}_6^{(j_m)}]^{(J)}\times$$
$$\times[\tilde{a}_3^{(j_n)}\times a_5^{(j_n)}]^{(J)}\Big]^{(0)}+(-1)^{x+k+k'}\,C_2\Big[[a_1^{(j_m)}\times\tilde{a}_6^{(j_m)}]^{(J_1)}\times$$
$$\times\Big[[a_4^{(j_n)}\times\tilde{a}_3^{(j_n)}]^{(x)}\times[\tilde{a}_2^{(j_n)}\times a_5^{(j_n)}]^{(J_2)}\Big]^{(J_1)}\Big]^{(0)}+C_3\sqrt{[j_n]}\times$$
$$\times\Big[[a_1^{(j_m)}\times\tilde{a}_6^{(j_m)}]^{(J)}\times[\tilde{a}_2^{(j_n)}\times a_5^{(j_n)}]^{(J)}\Big]^{(0)}\delta(x,0)\,\delta(k,k'), \tag{10}$$

where the multipliers C_1, C_2 and C_3 are the recoupling matrices that come from the recoupling of the tensorial products to the form given in Eq. (10).

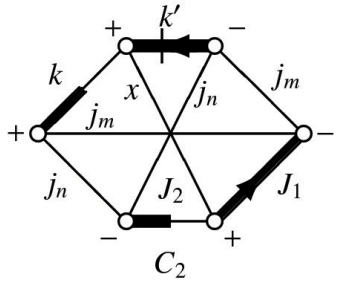

Fig. 4. Diagram showing the recoupling coefficient C_2.

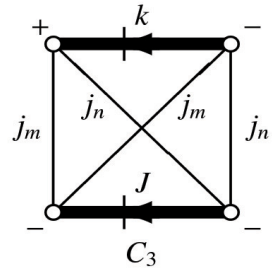

Fig. 5. Diagram showing the recoupling coefficient C_3.

Comparing the diagram B_1 from the paper [6] with the diagram C_1 of this paper, we see that in the diagram of this paper there is an arrow on the line j_n in the opposite direction and an opposite sign at the node (1). The rest is the same. Therefore, to have an analytical expression for the diagram C_1 in this paper, we only need to use the algebraic expression of the diagram B_1 in the paper [6], multiplied by the phase multiplier $(-1)^{2j_n}\times(-1)^{1+2j_n-x}\equiv(-1)^{1+x}$. The C_2 diagram is identical to the B_2 diagram from Ref. [6], i.e. $C_2\equiv B_2$, and C_3 is a new arrival. According to the graphical representation of angular momentum theory [20, 21], the diagram C_3 is equal to the 6-j symbol with additional multipliers. The algebraic expressions for C_1, C_2 and C_3 of these diagrams lead to the following analytical expression (10):

$$\Big[\Big[[a_1^{(j_m)}\times\tilde{a}_2^{(j_n)}]^{(k)}\times[\tilde{a}_3^{(j_n)}\times a_4^{(j_n)}]^{(x)}\Big]^{(k')}\times$$
$$\times[a_5^{(j_n)}\times\tilde{a}_6^{(j_m)}]^{(k')}\Big]^{(0)}=(-1)^{j_m+j_n+k'+x+1}\times$$
$$\times\sqrt{[k,k',x]}\begin{Bmatrix}j_m & j_n & k\\ x & k' & j_n\end{Bmatrix}\sum_J(-1)^J\sqrt{[J]}\begin{Bmatrix}j_m & j_m & J\\ j_n & j_n & k'\end{Bmatrix}\times$$
$$\times\Big[[a_1^{(j_m)}\times\tilde{a}_6^{(j_m)}]^{(J)}\times[\tilde{a}_3^{(j_n)}\times a_5^{(j_n)}]^{(J)}\Big]^{(0)}+$$
$$+(-1)^{j_m+j_n+k'}\sqrt{[k,k']}\sum_{J_1,J_2}\sqrt{[J_1,J_2]}\begin{Bmatrix}j_m & j_n & k\\ J_1 & J_2 & x\\ j_m & j_n & k'\end{Bmatrix}\times$$
$$\times\Big[[a_1^{(j_m)}\times\tilde{a}_6^{(j_m)}]^{(J_1)}\times\Big[[a_4^{(j_n)}\times\tilde{a}_3^{(j_n)}]^{(x)}\times$$
$$\times[\tilde{a}_2^{(j_n)}\times a_5^{(j_n)}]^{(J_2)}\Big]^{(J_1)}\Big]^{(0)}+$$
$$+\sqrt{[j_n,k]}\sum_J(-1)^J\sqrt{[J]}\begin{Bmatrix}j_m & j_m & J\\ j_n & j_n & k\end{Bmatrix}\times$$
$$\times\Big[[a_1^{(j_m)}\times\tilde{a}_6^{(j_m)}]^{(J)}\times[\tilde{a}_2^{(j_n)}\times a_5^{(j_n)}]^{(J)}\Big]^{(0)}\times$$
$$\times\,\delta(x,0)\,\delta(k,k'). \tag{11}$$

The first and the third terms in Eq. (11) correspond to the spin-angular part of the two-particle operators. The program library `librang` [15] is therefore sufficient for their calculation. The second term, with its three pairs of the second quantization operators, corresponds to the three-particle operator (6). In this case, we have succeeded in obtaining a tensorial expression for this three-particle operator for which the library `librang` [15] extension given in the paper [6] is sufficient (see Section 3.1 of the paper [6] for details). Only instead of Eq. (12) from the paper [6] we need to use the expression

$$\begin{aligned}&\left\langle (n_n\ell_n)j_n^w\alpha J\left\|\left[[a^{(j_n)}\times\tilde{a}^{(j_n)}]^{(x)}\times\right.\right.\right.\\&\left.\left.\left.\times[\tilde{a}^{(j_n)}\times a^{(j_n)}]^{(J_2)}\right]^{(J_1)}\right\|(n_n\ell_n)j_n^w\alpha' J'\right\rangle=\\&=(-1)^{J+J'+J_1}\sqrt{[J_1]}\sum_{\alpha'' J''}\begin{Bmatrix}x & J_2 & J_1\\ J' & J & J''\end{Bmatrix}\times\\&\times\left\langle (n_n\ell_n)j_n^w\alpha J\left\|[a^{(j_n)}\times\tilde{a}^{(j_n)}]^{(x)}\right\|(n_n\ell_n)j_n^w\alpha'' J''\right\rangle\times\\&\times\left\langle (n_n\ell_n)j_n^w\alpha'' J''\left\|[\tilde{a}^{(j_n)}\times a^{(j_n)}]^{(J_2)}\right\|(n_n\ell_n)j_n^w\alpha' J'\right\rangle.\end{aligned}\tag{12}$$

Therefore, the library `librang` must be extended by programming Eq. (12).

The above describes how to calculate the reduced matrix elements of a three-particle Feynman diagram CV_7 in the general case for the third type of core–valence correlations. But it is possible to extract the individual parts which are more straightforward to calculate, i.e. the coefficient $\Delta\varepsilon_0$ (does not depend on the term), $\Delta\mathcal{F}^k(n, n)$ and $\Delta\mathcal{F}^k(m, n)$ (regular spin-angular library `librang` can be used). The extraction of these expressions is the same as in the papers [2–6]. Therefore, only the reduced matrix element of part of Feynman diagrams A_5 with tensorial product (6) is calculated from the general expression when the rank $k > 0$. The part which is calculated from the general expression will be denoted by $\Delta\tilde{\tilde{\mathcal{R}}}^{(k,\,k',\,x)}(mnn)$ in the future.

3.2. The spin-angular part of the fourth type of core–valence correlations

Two different Feynman diagrams A_5 and A_6 from Fig. 2 describe this type of correlation. We will consider each separately, as their spin-angular part differs significantly.

3.2.1. The direct part of the fourth type of core–valence correlation

Now let us discuss the diagram A_5, with a tensorial structure

$$\begin{aligned}&\left[\left[[a_1^{(j_m)}\times\tilde{a}_2^{(j_n)}]^{(k)}\times[\tilde{a}_3^{(j_p)}\times a_4^{(j_p)}]^{(x)}\right]^{(k')}\times\right.\\&\left.\times[a_5^{(j_n)}\times\tilde{a}_6^{(j_m)}]^{(k')}\right]^{(0)}.\end{aligned}\tag{13}$$

As in Eq. (5), Eq. (13) is unsuitable to calculate the spin-angular part because there are two pairs of secondary quantization operators acting on different subshells, i.e. $[a_1^{(jm)}\times\tilde{a}_2^{(jn)}]^{(k)}$ and $[a_5^{(jn)}\times\tilde{a}_6^{(jm)}]^{(k)}$. Therefore, this tensorial product has to be transformed into the following, using the commutation rules of secondary quantization:

$$\begin{aligned}&\left[\left[[a_1^{(j_m)}\times\tilde{a}_6^{(j_m)}]^{(J_1)}\times[\tilde{a}_3^{(j_p)}\times a_4^{(j_p)}]^{(x)}\right]^{(J_2)}\times\right.\\&\left.\times[\tilde{a}_2^{(j_n)}\times a_5^{(j_n)}]^{(J_2)}\right]^{(0)}.\end{aligned}\tag{14}$$

But first of all, using the commutation rule (7) of secondary quantization we interchange the operators a_1 and a_2 and the operators a_5 and a_6. This leads to the expression

$$\begin{aligned}&\left[\left[[a_1^{(j_m)}\times\tilde{a}_2^{(j_n)}]^{(k)}\times[\tilde{a}_3^{(j_p)}\times a_4^{(j_p)}]^{(x)}\right]^{(k')}\times\right.\\&\left.\times[a_5^{(j_n)}\times\tilde{a}_6^{(j_m)}]^{(k')}\right]^{(0)}=\\&=(-1)^{k+k'}\left[\left[[\tilde{a}_2^{(j_n)}\times a_1^{(j_m)}]^{(k)}\times[\tilde{a}_3^{(j_p)}\times a_4^{(j_p)}]^{(x)}\right]^{(k')}\times\right.\\&\left.\times[\tilde{a}_6^{(j_m)}\times a_5^{(j_n)}]^{(k')}\right]^{(0)}.\end{aligned}\tag{15}$$

Now transforming the tensorial product (15) to (14) is determined by the tensorial product recoupling matrix, which is represented by the diagram B_3 from the paper [6] (see Fig. 5 there). The final result is

$$\begin{aligned}&\left[\left[[a_1^{(j_m)}\times\tilde{a}_2^{(j_n)}]^{(k)}\times[\tilde{a}_3^{(j_p)}\times a_4^{(j_p)}]^{(x)}\right]^{(k')}\times\right.\\&\left.\times[a_5^{(j_n)}\times\tilde{a}_6^{(j_m)}]^{(k')}\right]^{(0)}=\\&=(-1)^{k+k'}\sum_{J_1,J_2}B_3\left[\left[[a_1^{(j_m)}\times\tilde{a}_6^{(j_m)}]^{(J_1)}\times\right.\right.\\&\left.\left.\times[\tilde{a}_3^{(j_p)}\times a_4^{(j_p)}]^{(x)}\right]^{(J_2)}\times[\tilde{a}_2^{(j_n)}\times a_5^{(j_n)}]^{(J_2)}\right]^{(0)}=\end{aligned}\tag{16}$$

$$= (-1)^{j_m+j_n+k'+x}\sqrt{[k,k']}\sum_{J_1,J_2}\sqrt{[J_1,J_2]}\begin{Bmatrix} j_m & j_n & k \\ J_1 & J_2 & x \\ j_m & j_n & k' \end{Bmatrix}\times$$
$$\times\left[\left[[a_1^{(j_m)}\times\tilde{a}_6^{(j_m)}]^{(J_1)}\times[\tilde{a}_3^{(j_p)}\times a_4^{(j_p)}]^{(x)}\right]^{(J_2)}\times\right.$$
$$\left.\times[\tilde{a}_2^{(j_n)}\times a_5^{(j_n)}]^{(J_2)}\right]^{(0)}. \qquad \text{(16 continued)}$$

The program library `librang` [15] available in the GRASP package is sufficient for the calculation of the reduced matrix element of Feynman diagrams A_5, but the method of calculation of this type of operator is not described in Ref. [15]. This is described in the paper [6] (see Subsection 3.2.1 there).

3.2.2. The exchange part of the fourth type of core–valence correlations

Now let us discuss the diagram A_6, with a tensorial structure

$$\left[\left[[a_1^{(j_m)}\times\tilde{a}_2^{(j_n)}]^{(k)}\times[\tilde{a}_3^{(j_p)}\times a_4^{(j_n)}]^{(x)}\right]^{(k')}\times\right.$$
$$\left.\times[a_5^{(j_p)}\times\tilde{a}_6^{(j_m)}]^{(k')}\right]^{(0)}. \qquad (17)$$

This tensorial product is unsuitable to calculate the spin-angular part for the same reason as for Eqs. (5) and (13). Therefore, this tensorial product has to be transformed into the following, using the commutation rules of secondary quantization:

$$\left[\left[[a_1^{(j_m)}\times\tilde{a}_6^{(j_m)}]^{(J_1)}\times[\tilde{a}_3^{(j_p)}\times a_5^{(j_p)}]^{(y)}\right]^{(J_2)}\times\right.$$
$$\left.\times[\tilde{a}_2^{(j_n)}\times a_4^{(j_n)}]^{(J_2)}\right]^{(0)}. \qquad (18)$$

But first of all, using the commutation rule (7) of secondary quantization we interchange the operators a_1 and a_2 and the operators a_5 and a_6. This leads to the expression

$$\left[\left[[a_1^{(j_m)}\times\tilde{a}_2^{(j_n)}]^{(k)}\times[\tilde{a}_3^{(j_p)}\times a_4^{(j_n)}]^{(x)}\right]^{(k')}\times\right.$$
$$\left.\times[a_5^{(j_p)}\times\tilde{a}_6^{(j_m)}]^{(k')}\right]^{(0)} = (-1)^{j_n+j_p+k+k'+1}\times$$
$$\times\left[\left[[\tilde{a}_2^{(j_n)}\times a_1^{(j_m)}]^{(k)}\times[\tilde{a}_3^{(j_p)}\times a_4^{(j_n)}]^{(x)}\right]^{(k')}\times\right.$$
$$\left.\times[\tilde{a}_6^{(j_m)}\times a_5^{(j_p)}]^{(k')}\right]^{(0)}. \qquad (19)$$

Now transforming the tensorial product (19) to (18) is determined by the tensorial product recoupling matrix, which is represented by the diagram B_4 from the paper [6] (see Fig. 6 there). The final result is

$$\left[\left[[a_1^{(j_m)}\times\tilde{a}_2^{(j_n)}]^{(k)}\times[\tilde{a}_3^{(j_p)}\times a_4^{(j_n)}]^{(x)}\right]^{(k')}\times\right.$$
$$\left.\times[a_5^{(j_p)}\times\tilde{a}_6^{(j_m)}]^{(k')}\right]^{(0)} = (-1)^{j_n+j_p+k+k'+1}\times$$
$$\times\sum_{J_1,J_2,y}B_4\left[\left[[a_1^{(j_m)}\times\tilde{a}_6^{(j_m)}]^{(J_1)}\times[\tilde{a}_3^{(j_p)}\times a_5^{(j_p)}]^{(y)}\right]^{(J_2)}\times\right.$$
$$\left.\times[\tilde{a}_2^{(j_n)}\times a_4^{(j_n)}]^{(J_2)}\right]^{(0)} = (-1)^{j_m+j_n+k+1}\times$$
$$\times\sqrt{[k,k',x]}\sum_{J_1,J_2,y}(-1)^{J_1+J_2}\sqrt{[J_1,J_2,y]}\times$$
$$\times\left[\left[[a_1^{(j_m)}\times\tilde{a}_6^{(j_m)}]^{(J_1)}\times[\tilde{a}_3^{(j_p)}\times a_5^{(j_p)}]^{(y)}\right]^{(J_2)}\times\right.$$
$$\left.\times[\tilde{a}_2^{(j_n)}\times a_4^{(j_n)}]^{(J_2)}\right]^{(0)}\times \qquad (20)$$
$$\times\sum_z[z]\begin{Bmatrix} J_1 & j_n & z \\ j_n & y & J_2 \end{Bmatrix}\begin{Bmatrix} y & j_n & z \\ x & j_p & j_p \end{Bmatrix}\begin{Bmatrix} j_p & x & z \\ k & j_m & k' \end{Bmatrix}\begin{Bmatrix} j_m & k & z \\ j_n & J_1 & j_m \end{Bmatrix}.$$

The program library `librang` [15] available in the GRASP package is sufficient for the calculation of the reduced matrix element of Feynman diagram A_6. The use of the library in this case is exactly the same as the one presented in the paper [6] (see Subsection 3.2.2 there [6]). In this case, only the multiplier $\Theta'(n_i\lambda_i, n_j\lambda_j, n_i'\lambda_i', n_j'\lambda_j', \Xi)$ differs.

3.2.3. The special cases of the fourth type of core–valence correlations

The way to calculate reduced matrix elements of Feynman diagrams A_5 and A_6 in the general case is presented in Subsections 3.2.1 and 3.2.2. But it is possible to extract, as it was shown in Subsection 3.1, the individual parts which are more straightforward to calculate, i.e. the coefficient $\Delta\mathcal{E}_0$ (does not depend on the term) and $\Delta\mathcal{F}^k(n, p)$ (regular spin-angular library `librang` can be used). The extraction of these expressions is the same as in the papers [2–6]. Therefore, only the reduced matrix element of part of three-particle Feynman diagrams A_5 and A_6 is calculated from the general expression, where the rank $k > 0$. The part which is calculated from the general expression will be denoted by $\Delta\tilde{\tilde{\mathcal{R}}}^{(k,k',x)}(mnp)$ in the future.

In the next section, we will give the final expressions for these two types of correlations (third and fourth types of core–valence correlations), as we did in the papers [2–6].

4. Combination of RCI approximation with the stationary second-order Rayleigh–Schrödinger many-body perturbation theory

Similar to core–valence [2], core [3], core–core [4], and valence–valence [5, 6] correlations the admixed configurations from core–valence correlations deriving from the three-particle Feynman diagram CV_7 (Eqs. (1) and (4)) can be added to the usual energy $E_0(K)$ of the term χJ of the configuration K and can be expressed as the energy $\Delta\varepsilon_0(KJ)$, which does not depend on the term, and the sum of the product of Slater integrals and spin-angular coefficients, describing the interaction within and between open subshells,

$$
\begin{aligned}
&E(K\chi J) = E_0(KJ) + \Delta\varepsilon_0(KJ) + \\
&+\sum_{n\ell j}\sum_{k>0} \tilde{f}_k(\ell j^w, K\chi J)[\,\mathcal{F}^k(n\ell j, n\ell j) + \\
&+\Delta\mathcal{F}^k(n\ell j, n\ell j)] + \\
&+\sum_{n\ell j}\sum_{n'\ell'j'>n\ell j}\left\{\sum_{k>0}\tilde{f}_k(\ell j^w\ell'j'^{w'}, K\chi J)\times\right. \\
&\times[\,\mathcal{F}^k(n\ell j, n'\ell'j') + \Delta\mathcal{F}^k(n\ell j, n'\ell'j')] \; + \\
&+\sum_k \tilde{g}_k(\ell j^w\ell'j'^{w'}, K\chi J)\;\mathcal{G}^k(n\ell j, n'\ell'j') + \\
&+\sum_k \tilde{v}_k(\ell j^w\ell'j'^{w'},\; \ell j^{w-2}\ell'j'^{w'+2},\; K\chi JK'\chi' J)\times \\
&\left.\times\;\mathcal{R}^k(n\ell jn\ell j, n'\ell'j'n'\ell'j')\right\} + \\
&+\sum_{\substack{n\ell j\\ n'\ell'j'\neq n\ell j}}\sum_{\substack{k>0\\ k',x}}\left\langle\Psi\middle\|\left[[a^{(j)}\times\tilde{a}^{(j)}]^{(k)}\times\right.\right. \\
&\left.\left.\times\left[[a^{(j')}\times\tilde{a}^{(j')}]^{(x)}\times[\tilde{a}^{(j')}\times a^{(j')}]^{(k')}\right]^{(k)}\right]^{(0)}\middle\|\Psi\right\rangle\times \\
&\times\Delta\tilde{\tilde{\mathcal{R}}}^{(k,k',x)}(n\ell\, j\, n'\ell'j'n'\ell'j') + \\
&+\sum_{\substack{n\ell j\\ n'\ell'j'\neq n\ell j\\ n''\ell''j''\neq n\ell j}}\sum_{\substack{k>0\\ k',x}}\left\langle\Psi\middle\|\left[\left[[a^{(j)}\times\tilde{a}^{(j)}]^{(k)}\times\right.\right.\right. \\
&\left.\left.\left.\times[\tilde{a}^{(j'')}\times a^{(j'')}]^{(x)}\right]^{(k')}\times[\tilde{a}^{(j')}\times a^{(j')}]^{(k')}\right]^{(0)}\middle\|\Psi\right\rangle\times \\
&\times\Delta\tilde{\tilde{\mathcal{R}}}^{(k,k',x)}(n\ell\, j\, n'\ell'j'n''\ell''j''),
\end{aligned}
\tag{21}
$$

where $\tilde{f}_k$, $\tilde{g}_k$ and $\tilde{v}_k$ are spin-angular coefficients from which submatrix elements $\langle\ell j\|C^{(k)}\|\ell'j'\rangle$ are extracted. Therefore, the summation over k runs over all possible values instead of the values that satisfy the triangular condition $(\ell\ell'k)$ as it is in the regular case. The $\mathcal{F}^k(n\ell j, n'\ell'j')$, $\mathcal{G}^k(n\ell j, n'\ell'j')$ and $\mathcal{R}^k(n\ell jn\ell j, n'\ell'j'n'\ell'j')$ are the generalized integrals of the electrostatic interaction between electrons. The definition of $\mathcal{R}^k(n\ell jn\ell j, n'\ell'j'n'\ell'j')$ is the following:

$$
\begin{aligned}
&\mathcal{R}^k(ij, i'j') = \\
&=\{[1+\delta(i,j)]\,[1+\delta(i',j')]\}^{-1/2}\times R^k(n_ij_in_jj_j, n_{i'}j_{i'}n_{j'}j_{j'})\times \\
&\times\langle\ell_ij_i\|C^{(k)}\|\ell_{i'}j_{i'}\rangle\,\langle\ell_jj_j\|C^{(k)}\|\ell_{j'}j_{j'}\rangle,
\end{aligned}
\tag{22}
$$

where $R^k(n_ij_in_jj_j, n_{i'}j_{i'}n_{j'}j_{j'})$ is the same radial integral as in Eq. (3). Definitions $\mathcal{F}^k(n\ell j, n'\ell'j')$ and $\mathcal{G}^k(n\ell j, n'\ell'j')$ straightforwardly follow from Eq. (22). Due to the inherent complexity of the three-particle operator, Eq. (21) does not fully distinguish all the members that are independent of the term. Therefore, a very small number of them are retained in the members $\Delta\mathcal{F}^k(n\ell j, n\ell j)$, $\Delta\tilde{\tilde{\mathcal{R}}}^{(k,k',x)}(n\ell j\, n'\ell'j'\, n'\ell'j')$ and $\Delta\tilde{\tilde{\mathcal{R}}}^{(k,k',x)}(n\ell j\, n'\ell'j'\, n''\ell''j'')$.

The contribution deriving from the core–valence correlations of the configurations K' to $E(K\chi J)$ in the second-order of the perturbation theory can be extracted from Eq. (21) as

$$
\begin{aligned}
&\Delta E_{\mathrm{PT(CVT)}} = \Delta\varepsilon_0(KJ) + \\
&+\sum_{n\ell j}\sum_{k>0}\tilde{f}_k(\ell j^w, K\chi J)\Delta\,\mathcal{F}^k(n\ell j, n\ell j) + \\
&+\sum_{n\ell j}\sum_{n'\ell'j'>n\ell j}\sum_{k>0}\tilde{f}_k(\ell j^w\ell'j'^{w'}, K\chi J)\,\Delta\mathcal{F}^k(n\ell j, n'\ell'j') + \\
&+\sum_{\substack{n\ell j\\ n'\ell'j'\neq n\ell j}}\sum_{\substack{k>0\\ k',x}}\left\langle\Psi\middle\|\left[[a^{(j)}\times\tilde{a}^{(j)}]^{(k)}\times\left[[a^{(j')}\times\tilde{a}^{(j')}]^{(x)}\times\right.\right.\right. \\
&\left.\left.\left.\times[\tilde{a}^{(j')}\times a^{(j')}]^{(k')}\right]^{(k)}\right]^{(0)}\middle\|\Psi\right\rangle\times \\
&\times\Delta\tilde{\tilde{\mathcal{R}}}^{(k,k',x)}(n\ell jn'\ell'j'n'\ell'j') + \\
&+\sum_{\substack{n\ell j\\ n'\ell'j'\neq n\ell j\\ n''\ell''j''\neq n\ell j}}\sum_{\substack{k>0\\ k',x}}\left\langle\Psi\middle\|\left[\left[[a^{(j)}\times\tilde{a}^{(j)}]^{(k)}\times[\tilde{a}^{(j'')}\times a^{(j'')}]^{(x)}\right]^{(k')}\times\right.\right. \\
&\left.\left.\times[\tilde{a}^{(j')}\times a^{(j')}]^{(k')}\right]^{(0)}\middle\|\Psi\right\rangle\times \\
&\times\Delta\tilde{\tilde{\mathcal{R}}}^{(k,k',x)}(n\ell jn'\ell'j'n''\ell''j'').
\end{aligned}
\tag{23}
$$

The contribution of the third and fourth type of the core–valence correlations in the second-order of the perturbation theory is expressed over $\Delta\mathcal{E}_0$ (KJ), $\Delta\mathcal{F}^k(n\ell j,\ n\ell j)$, $\Delta\mathcal{F}^k(n\ell j,\ n'\ell' j')$, $\Delta\widetilde{\widetilde{\mathcal{R}}}^{(k,\ k',\ x)}$ ($n\ell jn'\ell' j'$ $n'\ell' j'$) and $\Delta\widetilde{\widetilde{\mathcal{R}}}^{(k,\ k',\ x)}$ ($n\ell j\ n'\ell' j'n''\ell'' j''$) (see Tables 1, 2 and 3). These formulae are additionally expressed via the quantities

$$\mathcal{A}'(x,ij,i'j') = \\ = \sum_{k,k'} \begin{Bmatrix} k & k' & x \\ j_i & j_i & j_{i'} \end{Bmatrix} \begin{Bmatrix} k & k' & x \\ j_j & j_j & j_{j'} \end{Bmatrix} \mathcal{P}(kk',ij,i'j'), \quad (24)$$

$$\mathcal{C}(k,ij,i'j') = \sum_{k'} \begin{Bmatrix} k & j_i & j_{i'} \\ k' & j_j & j_{j'} \end{Bmatrix} Q(kk',ij,i'j'), \quad (25)$$

and

$$\mathcal{G}'(x_1x_2x,ij,i'j') = \\ = \sum_{k,k'} (-1)^{k'} \begin{Bmatrix} j_{j'} & j_{j'} & x \\ k & k' & j_j \end{Bmatrix} \begin{Bmatrix} j_i & j_{i'} & k \\ x_1 & x_2 & x \\ j_i & j_{i'} & k' \end{Bmatrix} \mathcal{P}(kk',ij,i'j'), \quad (26)$$

where

$$\mathcal{P}(kk',ij,i'j') = \mathcal{R}^k(ij,i'j')\,\mathcal{R}^{k'}(i'j',ij)\,\mathcal{O}(K',K), \quad (27)$$

$$Q(kk',ij,i'j') = \mathcal{R}^k(ij,i'j')\,\mathcal{R}^{k'}(i'j',ji)\,\mathcal{O}(K',K), \quad (28)$$

$$\mathcal{O}(K',K) = \frac{1}{\bar{E}(K') - \bar{E}(K)}, \quad (29)$$

where $\bar{E}(K)$ is the averaged energy of the state for which calculations are performed. $\bar{E}(K')$ is the averaged energy for the admixed configuration K'. For details on how to find $\bar{E}(K)$ and $\bar{E}(K')$, see Ref. [2], Section 3 therein. We would also like to emphasize that the energy denominator (29) is defined differently/opposite to the expressions of Feynman diagrams (see Fig. 1, Eqs. (27, 28)).

$$\mathcal{C}_{12j}(iji',k_1k_2k_3,J_1J_2J) = \\ = \sum_x [x] \begin{Bmatrix} J_1 & j_j & x \\ j_j & J & J_2 \end{Bmatrix} \begin{Bmatrix} J & j_j & x \\ k_3 & j_{i'} & j_{i'} \end{Bmatrix} \times \\ \times \begin{Bmatrix} j_{i'} & k_3 & x \\ k_1 & j_i & k_2 \end{Bmatrix} \begin{Bmatrix} j_i & k_1 & x \\ j_j & J_1 & j_i \end{Bmatrix}. \quad (30)$$

We would also like to point out that the notation of ranks such as J_1, J_2, y in the multipliers of this section under $\Delta\widetilde{\widetilde{\mathcal{R}}}^{(k,k',x)}$ (mnn) and $\Delta\widetilde{\widetilde{\mathcal{R}}}^{(k,k',x)}$ (mnp) have been renamed for convenience to make the expressions in Tables 2 and 3 more straightforward and more understandable.

This theory in an irreducible tensorial form, as in the papers [2–6], is more suitable to be included in such a version of the GRASP which is based on conuration state function generators [8, 22]. This is related to the fact that this version of the software package allows us to easily distinguish F, F' and G sets of orbitals in the process of computing atomic data. In the following section, we will present a test case of this implementation.

Table 1. Expressions for core–valence corrections to the energy in Eqs. (21) and (23), independent of the term.

$\Delta\mathcal{E}_0$ corrections
$\overbrace{(n_a\ell_a)j_a^{2j_a+1}}^{\text{core subshell}}\ \overbrace{(n_m\ell_m)j_m^{w_m}(n_n\ell_n)j_n^{w_n}}^{\text{valence subshells}} \to \overbrace{(n_a\ell_a)j_a^{2j_a}}^{\text{core subshell}}\ \overbrace{(n_m\ell_m)j_m^{w_m-1}(n_n\ell_n)j_n^{w_n+2}}^{\text{valence subshells}}$
$\underbrace{2(-1)^{j_m+j_a}\,\frac{w_m([j_n]-2w_n)}{[j_m,j_n]}\sum_k\left\{\mathcal{C}(k,nn,am)+\frac{1}{[k]}\mathcal{P}(kk,ma,nn)\right\}}_{\text{from CV}_7\ \text{Feynman diagram}}$
$\overbrace{(n_a\ell_a)j_a^{2j_a+1}}^{\text{core subshell}}\ \overbrace{(n_m\ell_m)j_m^{w_m}(n_n\ell_n)j_n^{w_n}(n_p\ell_p)j_p^{w_p}}^{\text{valence subshells}} \to \overbrace{(n_a\ell_a)j_a^{2j_a}}^{\text{core subshell}}\ \overbrace{(n_m\ell_m)j_m^{w_m-1}(n_n\ell_n)j_n^{w_n+1}(n_p\ell_p)j_p^{w_p+1}}^{\text{valence subshells}}$
$\underbrace{-(-1)^{j_m+j_n+j_p+j_a}\,\frac{w_m([j_n]-w_n)([j_p]-w_p)}{[j_m,j_n,j_p]}\sum_k\left\{\frac{\mathcal{P}(kk,ma,np)}{[k]}+\mathcal{C}(k,ma,np)\right\}(1+\mathrm{P}(n\rightleftharpoons p))}_{\text{from CV}_7\ \text{Feynman diagram}}$

Table 2. Expressions for Slater integral $\Delta\mathcal{F}^k(n, n)$ and $\Delta\mathcal{F}^k(m, n)$, and $\Delta\tilde{\tilde{\mathcal{R}}}^{(k,k',x)}$ (mnn) (see Eqs. (21, 23)) corrections corresponding to the third type of core–valence correlations.

Corrections	Slater integral	k values
$\overbrace{(n_a\ell_a)j_a^{2j_a+1}}^{\text{core subshell}}\overbrace{(n_m\ell_m)j_m^{w_m}(n_n\ell_n)j_n^{w_n}}^{\text{valence subshells}} \to \overbrace{(n_a\ell_a)j_a^{2j_a}}^{\text{core subshell}}\overbrace{(n_m\ell_m)j_m^{w_m-1}(n_n\ell_n)j_n^{w_n+2}}^{\text{valence subshells}}$		
$\underbrace{-4\frac{[k]}{[j_m]}w_m\mathcal{A}'(k,nn,ma)}_{\text{from CV}_7\text{ Feynman diagram}}$	$\Delta\mathcal{F}^k(n, n)$	$k \geq 0$
$\underbrace{2[k]\sum_{k'}(-1)^{j_n+j_a+k'}\begin{Bmatrix} j_m & j_m & k \\ j_n & j_n & k' \end{Bmatrix}\times}_{\text{from CV}_7\text{ Feynman diagram}}$	$\Delta\mathcal{F}^k(m, n)$	$k > 0$
$\underbrace{\times\left\{\mathcal{C}(k',nn,am)+\frac{1}{[k']}\mathcal{P}(k'k',ma,nn)\right\}}_{\text{from CV}_7\text{ Feynman diagram}}$		
$\underbrace{2(-1)^{j_m+j_n}\sqrt{[k,k',x]}\ \mathcal{G}'(kk'x,nn,ma)}_{\text{from CV}_7\text{ Feynman diagram}}$	$\Delta\tilde{\tilde{\mathcal{R}}}^{(k,k',x)}(mnn)$	$k > 0$

Table 3. Expressions for Slater integral $\Delta\mathcal{F}^k(n, p)$ and $\Delta\tilde{\tilde{\mathcal{R}}}^{(k,k',x)}$ (mnp) (see Eqs. (21, 23)) corrections corresponding to the fourth type of core-valence correlations.

Corrections	Slater integral	k values
$\overbrace{(n_a\ell_a)j_a^{2j_a+1}}^{\text{core subshell}}\overbrace{(n_m\ell_m)j_m^{w_m}(n_n\ell_n)j_n^{w_n}(n_p\ell_p)j_p^{w_p}}^{\text{valence subshells}} \to \overbrace{(n_a\ell_a)j_a^{2j_a}}^{\text{core subshell}}\overbrace{(n_m\ell_m)j_m^{w_m-1}(n_n\ell_n)j_n^{w_n+1}(n_p\ell_p)j_p^{w_p+1}}^{\text{valence subshells}}$		
$\underbrace{(-1)^{j_m+j_n}[k]\sqrt{[k]}\frac{w_m}{\sqrt{[j_m]}}\left\{(-1)^{k+1}\mathcal{G}'(0kk,ma,np)+\right.}_{\text{from CV}_7\text{ Feynman diagram}}$	$\Delta\mathcal{F}^k(n, p)$	$k > 0$
$\underbrace{+\sum_{k_1,k_2,k_3}(-1)^{k_1+k}[k_3]\begin{Bmatrix} j_n & j_p & k_3 \\ k_1 & k_2 & j_a \end{Bmatrix}Q(k_1k_2,ma,np)\times}_{\text{from CV}_7\text{ Feynman diagram}}$		
$\underbrace{\times\ \mathcal{C}_{12j}(j_mj_nj_p,k_1k_2k_3,0kk)\left\}\left(1+\mathrm{P}\begin{pmatrix} n\rightleftharpoons p \\ k_1\rightleftharpoons k_2 \end{pmatrix}\right)\right.}_{\text{from CV}_7\text{ Feynman diagram}}$		
$\underbrace{-(-1)^{j_m+j_n}\sqrt{[k,k',x]}\left\{(-1)^{x+1}\mathcal{G}'(kk'x,ma,np)+\right.}_{\text{from CV}_7\text{ Feynman diagram}}$	$\Delta\tilde{\tilde{\mathcal{R}}}^{(k,k',x)}(mnp)$	$k > 0$
$\underbrace{+\sum_{k_1,k_2,k_3}(-1)^{k+k'+k_1}[k_3]\begin{Bmatrix} j_n & j_p & k_3 \\ k_1 & k_2 & j_a \end{Bmatrix}Q(k_1k_2,ma,np)\times}_{\text{from CV}_7\text{ Feynman diagram}}$		
$\underbrace{\times\ \mathcal{C}_{12j}(j_mj_nj_p,k_1k_2k_3,kk'x)\left\}\left(1+\mathrm{P}\begin{pmatrix} n\rightleftharpoons p \\ k_1\rightleftharpoons k_2 \\ k'\rightleftharpoons x \end{pmatrix}\right)\right.}_{\text{from CV}_7\text{ Feynman diagram}}$		

5. Calculation of core–valence, core, core–core and valence–valence with a new approach

In the present work, the method, based on the Rayleigh–Schrödinger perturbation theory in an irreducible tensorial form [2–6], is extended to include the CV correlations of third and fourth types in the computations. We performed MCDHF calculations using the regular method and later using the RSMBPT method, the CV, C, CC and VV correlations are included in the RCI computations. For this purpose, we computed the lifetime of the $2s2p^6\ ^2S_{1/2}$ state and the 12 lowest energy levels of the $2s^22p^5$, $2s2p^6$ and $2s^22p^4\{3s,3p\}$ configurations of Ne II. To find the lifetime, only states with $J = 1/2$ and $3/2$ for the odd configurations and states with $J = 1/2$ for the even configurations are needed. The multireference (MR) set in the present calculations consists of the $2s2p^6$, $2s^22p^4\{3s,3d\}$, $2s2p^4\{3s^2,3d^2\}$, $2s^22p^33p3d$ and $2s^22p^33s3p$ even as well as $2s^22p^5$, $2s^22p^43p$, $2p^43s^23p$ and $2p^43p3d^2$ odd configurations. It should be noted that the MR set in the present computations consists of orbitals with few different principal quantum numbers, namely with n and $n + 1$ (where $n = 2$).

5.1. Computational schemes

The regular MCDHF method was used to calculate the radial wave functions of the orbitals in the MR configurations, and later the radial functions of the virtual orbitals. Only VV correlations were included in this computational scheme and it is marked **VV MCDHF**. Single–double (SD) substitutions are allowed from 2s, 2p$_-$, 2p, 3s, 3p$_-$, 3p, 3d$_-$ and 3d valence orbitals of the MR set to the virtual orbital set (OS) $OS_1 = \{4s, .., 4l_{max}\}$, ... and $OS_5 = \{8s, .., 8l_{max}\}$. Three l_{max} values were tested: l_{max} = d, f, g in this scheme. At the RCI stage, the CV, C and CC correlations were added to the investigation, where the 1s orbital is defined as the core. This computation scheme was named **RCI [w VV]**.

The second set of radial functions was computed, including VV and C correlations, where the 1s orbital is also defined as the core. This computation is marked as **VV+C MCDHF**. Sets of virtual orbitals were restricted up to l_{max} = g. At the RCI stage, the CV, C and CC correlations were added to the investigation as in the previous case, and this scheme was named as **RCI[w VV+C]**.

The next investigations were done using the RSMBPT method at the RCI computation. The CSF space in this method is divided into three sets: *F*, *F′* and *G* (see Ref. [2] for details). The 1s subshell is defined as a core subshell (that corresponds to the *F* set), 2s, 2p$_-$, 2p, 3s, 3p$_-$, 3p, 3d$_-$ and 3d as valence subshells (that correspond to the *F′* set) and sub-shells belonging to OS_1, ... and OS_5 as virtual ones (that correspond to the *G* set). The l_{max} of virtual orbitals is described as in the **VV MCDHF** method. This space distribution is consistent with regular Grasp2018 calculations and allows the use of a combination of RCI and RSMBPT methods.

The RSMBPT calculation procedure for RCI is analogous to that used in the previous research [2–6]. Using radial functions from the **VV MCDHF** method, the contribution of each *K′* configuration for CSF in the MR set was calculated according to Rayleigh–Schrödinger perturbation theory in an irreducible tensorial form, is computed according to Eq. (22) of Ref. [2] (for first and second types of CV correlations), Eq. (6) of Ref. [3] (for C correlations), Eq. (26) of Ref. [4] (for CC correlations), Eq. (19) of Ref. [5] (for first and second types VV correlations), Eq. (26) of Ref. [6] (for third and fourth VV correlations) and Eq. (23) (for third and fourth types of CV correlations). *K′* configurations are sorted in a descending order according to the impact of the correlations for each CSF in the MR set. Further, *K′* configurations are selected by the impact of CV, C, CC and VV correlations with the specified fraction (expressed in the percentage: 95, 99, 99.5, 99.95 and 100%) of the total correlations contribution, and then the RCI method was applied, including them. It should be noted that the program gives the contribution of the correlations of *K′* configuration with a value greater than `1.0E-11`. Contributions of smaller magnitudes are neglected. The C correlations (Eq. (3) of Ref. [3]) and V correlations, which are not included in the RSMBPT method, were added to the RCI calculations in a regular way. This computation scheme is named as **RCI (RSMBPT)[w VV]**.

The RCI (RSMBPT) computation was repeated using the radial function from the **VV+C MCDHF** scheme. This scheme was named as **RCI (RSMBPT) [w VV+C]**.

5.2. Results

5.2.1. Energy levels

Table 4 presents the energy levels recommended by the NIST ASD [23] and the relative differences $(E_{NIST} - E)/E_{NIST}$ between our computed energy levels and the NIST ASD-recommended values for the 12 lowest energy levels of the $2s2p^6$, $2s^22p^5$ and $2s^22p^4\{3s, 3p\}$ configurations. Three atomic states involved in the transition that affects lifetimes are highlighted. The energy levels calculated using the standard **RCI [w VV]** method are presented for the OS_5 virtual orbital set. This set is also restricted by orbital symmetry (l_{max} = d, f, g), and the results from each of them are given in the Table. The same Table shows the results of further calculations using the RSMBPT method. Using that method, the specified amount (95, 99, 99.5, 99.95 and 100%) of CV, C, CC and VV correlations (**RCI (RSMBPT)**) was included in the RCI step. Those correlations were included up to the virtual orbital sets OS_5, constrained by orbital symmetry as in the case of the above MCDHF method. Similarly, the relative differences between the NIST recommended energy levels and energy levels obtained using the regular **RCI [w VV+C]** and **RCI (RSMBPT) [w VV+C]** methods are presented for the OS_5 virtual orbital set with the orbital symmetry l_{max} = g. The root-mean-square (*rms*) deviation of all levels and those three levels (rms_3) involved in the transitions depopulating the $2s2p^6\ ^2S_{1/2}$ atomic state are given for all these schemes in Table 4.

Table 4. Energy levels (in cm^{-1}) from NIST ASD (E_{NIST}), relative differences $(E_{NIST}–E)/E_{NIST}$ (in %) from NIST ASD and our computed energy levels using regular **RCI[w VV]** (a), **RCI[w VV+C]** (b) methods, and **RCI (RSMBPT)[w VV]**, **RCI (RSMBPT) [w VV+C]**, root-mean square deviations *rms* and rms_3 (in cm^{-1}) of all computed levels and of three atomic states involved in the transition that affects lifetime; these states are highlighted.

ASF	E_{NIST}	$(E_{NIST} - E)/E_{NIST}$										
		a	b	**RCI (RSMBPT)[w VV]**					**RCI (RSMBPT)[w VV+C]**				
				95%	99%	99.5%	99.95%	100%	95%	99%	99.5%	99.95%	100%
						l_{max} = d							
$2s^22p^5\ ^2P^o_{3/2}$	0												
$2s^22p^4(^3P)3p\ ^4P^o_{3/2}$	246415	0.93		1.01	0.93	0.92	0.93	0.93					
$2s^22p^4(^3P)3p\ ^4D^o_{3/2}$	249696	0.80		0.88	0.80	0.80	0.80	0.80					
$2s^22p^4(^3P)3p\ ^2D^o_{3/2}$	251522	0.52		0.57	0.50	0.50	0.51	0.52					
$2s^22p^5\ ^2P^o_{1/2}$	780	1.83		–1.77	–0.47	1.43	2.49	1.70					
$2s^22p^4(^3P)3p\ ^4P^o_{1/2}$	246598	0.94		1.04	0.94	0.93	0.93	0.93					
$2s^22p^4(^3P)3p\ ^4D^o_{1/2}$	249840	0.82		0.89	0.82	0.82	0.82	0.82					
$2s^22p^4(^3P)3p\ ^2S^o_{1/2}$	252798	0.49		0.52	0.46	0.47	0.48	0.49					
$2s2p^6\ ^2S_{1/2}$	217048	1.27		1.34	1.28	1.28	1.28	1.27					
$2s^22p^4(^3P)3s\ ^4P_{1/2}$	219947	2.00		2.18	2.04	2.02	2.00	2.01					
$2s^22p^4(^3P)3s\ ^2P_{1/2}$	224699	1.89		2.08	1.93	1.91	1.89	1.89					
$2s^22p^4(^1S)3s\ ^2S_{1/2}$	276677	1.18		1.27	1.17	1.16	1.16	1.16					
rms		2546		2771	2564	2548	2538	2536					
rms_3		1597		1673	1608	1608	1603	1595					
						l_{max} = f							
$2s^22p^5\ ^2P^o_{3/2}$	0												
$2s^22p^4(^3P)3p\ ^4P^o_{3/2}$	246415	0.23		0.32	0.23	0.23	0.22	0.23					
$2s^22p^4(^3P)3p\ ^4D^o_{3/2}$	249696	0.17		0.25	0.17	0.17	0.16	0.16					
$2s^22p^4(^3P)3p\ ^2D^o_{3/2}$	251522	–0.13		–0.07	–0.15	–0.15	–0.14	–0.14					
$2s^22p^5\ ^2P^o_{1/2}$	780	1.74		–3.89	–0.01	–0.01	2.49	1.69					
$2s^22p^4(^3P)3p\ ^4P^o_{1/2}$	246598	0.24		0.35	0.24	0.24	0.23	0.23					
$2s^22p^4(^3P)3p\ ^4D^o_{1/2}$	249840	0.20		0.26	0.19	0.19	0.19	0.19					
$2s^22p^4(^3P)3p\ ^2S^o_{1/2}$	252798	–0.10		–0.07	–0.13	–0.13	–0.12	–0.11					

Table 4. (continued)

ASF	E_{NIST}	$(E_{NIST} - E)/E_{NIST}$											
		a	b	**RCI (RSMBPT) [w VV]**					**RCI (RSMBPT) [w VV+C]**				
				95%	99%	99.5%	99.95%	100%	95%	99%	99.5%	99.95%	100%
$2s2p^6\ ^2S_{1/2}$	217048	0.71		0.75	0.71	0.71	0.70	0.70					
$2s^22p^4(^3P)3s\ ^4P_{1/2}$	219947	1.31		1.50	1.36	1.36	1.31	1.30					
$2s^22p^4(^3P)3s\ ^2P_{1/2}$	224699	1.26		1.45	1.30	1.30	1.25	1.24					
$2s^22p^4(^1S)3s\ ^2S_{1/2}$	276677	0.63		0.71	0.61	0.61	0.59	0.60					
rms		1383		1590	1415	1386	1366	1363					
rms_3		888		938	890	883	878	876					
						l_{max} = g							
$2s^22p^5\ ^2P^o_{3/2}$	0												
$2s^22p^4(^3P)3p\ ^4P^o_{3/2}$	246415	−0.07	−0.07	0.04	−0.06	−0.08	−0.08	−0.08	0.03	−0.06	−0.08	−0.08	−0.08
$2s^22p^4(^3P)3p\ ^4D^o_{3/2}$	249696	−0.13	−0.13	−0.02	−0.12	−0.13	−0.13	−0.13	−0.03	−0.12	−0.13	−0.14	−0.13
$2s^22p^4(^3P)3p\ ^2D^o_{3/2}$	251522	−0.43	−0.43	−0.35	−0.43	−0.44	−0.44	−0.43	−0.36	−0.43	−0.44	−0.44	−0.44
$2s^22p^5\ ^2P^o_{1/2}$	780	1.65	1.61	−5.86	0.54	0.61	2.79	1.60	−6.56	0.68	−1.24	2.63	1.57
$2s^22p^4(^3P)3p\ ^4P^o_{1/2}$	246598	−0.06	−0.06	0.06	−0.05	−0.06	−0.07	−0.07	0.06	−0.05	−0.06	−0.07	−0.07
$2s^22p^4(^3P)3p\ ^4D^o_{1/2}$	249840	−0.10	−0.10	−0.02	−0.09	−0.10	−0.11	−0.11	−0.03	−0.09	−0.10	−0.11	−0.11
$2s^22p^4(^3P)3p\ ^2S^o_{1/2}$	252798	−0.40	−0.41	−0.35	−0.42	−0.43	−0.42	−0.42	−0.36	−0.42	−0.43	−0.42	−0.42
$2s2p^6\ ^2S_{1/2}$	217048	0.67	0.80	0.72	0.68	0.67	0.66	0.66	0.84	0.81	0.80	0.80	0.79
$2s^22p^4(^3P)3s\ ^4P_{1/2}$	219947	0.96	1.09	1.16	1.01	0.98	0.96	0.95	1.28	1.14	1.12	1.09	1.08
$2s^22p^4(^3P)3s\ ^2P_{1/2}$	224699	0.92	1.05	1.13	0.97	0.94	0.92	0.91	1.24	1.10	1.07	1.04	1.03
$2s^22p^4(^1S)3s\ ^2S_{1/2}$	276677	0.45	0.55	0.53	0.43	0.42	0.41	0.42	0.62	0.53	0.52	0.50	0.52
rms		1111	1260	1265	1150	1128	1104	1096	1403	1296	1276	1252	1244
rms_3		836	1003	901	854	837	831	825	1054	1019	1005	999	992

The conclusion is that the RCI (RSMBPT) method reproduces regular RCI energy levels independently of the orbital symmetry of virtual orbitals (see line 100%). In addition, the ability of the RCI (RSMBPT) method to reproduce energy levels is independent of the type of correlations included in the regular MCDHF computations of radial wave functions (see the line 100% of **RCI (RSMBPT) [w VV+C]** column). It should be noted that, for this ion, the RCI (RSMBPT) method already reproduces the regular RCI results for most energy levels when 99.5% of the correlations are included; only the $2s^22p^5\ ^2P^o_{1/2}$ level requires full (100%) correlation inclusion.

Figure 6 illustrates the contribution of the included correlations (Δ_{cor}) obtained using the RCI (RSMBPT) method, relative to the complete standard RCI calculations, as a function of the fraction of the total correlation contribution included in the RCI (RSMBPT) approach. This dependence is shown for the $2s^22p^5\ ^2P^o_{3/2}$, $2s^22p^5\ ^2P^o_{1/2}$ and $2s2p^6\ ^2S_{1/2}$ levels when CV, C, CC and VV correlations are taken into account. The same dependence is presented for each tested orbital symmetry of the virtual space, l_{max} = d, f, g, and for the radial wave functions computed with VV+C correlations included. The contribution Δ_{cor} (in %) is defined as $(TE_{\mathbf{RCI(RSMBPT)}} - TE_{\mathbf{MR+}})/(TE_{\mathbf{RCI}} - TE_{\mathbf{MR+}})$, where TE denotes the total energy obtained within a given computational scheme. Here, $TE_{\mathbf{RCI(RSMBPT)}}$ is the total energy calculated using the RCI (RSMBPT) method with a specified fraction (in %) of the total correlation contribution included. The $TE_{\mathbf{MR+}}$ values are obtained from the calculations in which the CSF basis consists of the MR set augmented by correlation effects not included in the RSMBPT method. As can be observed in the Figure, the computed Δ_{cor} is almost identical to the specified fraction (in %) of the total correlations contribution used in the RCI (RSMBPT) method, exhibiting a linear dependence, independent of the orbital symmetry and the correlations included in the radial function calculations. The linear fitting ($y = kx + a$) demonstrates that the slope coefficient (k) is less than unity, ranging from 0.74 to 0.85, and that the error associated with the fitting itself is negligible compared to the resulting values (see Fig. 6), indicating that the k-factor is highly precise. Based

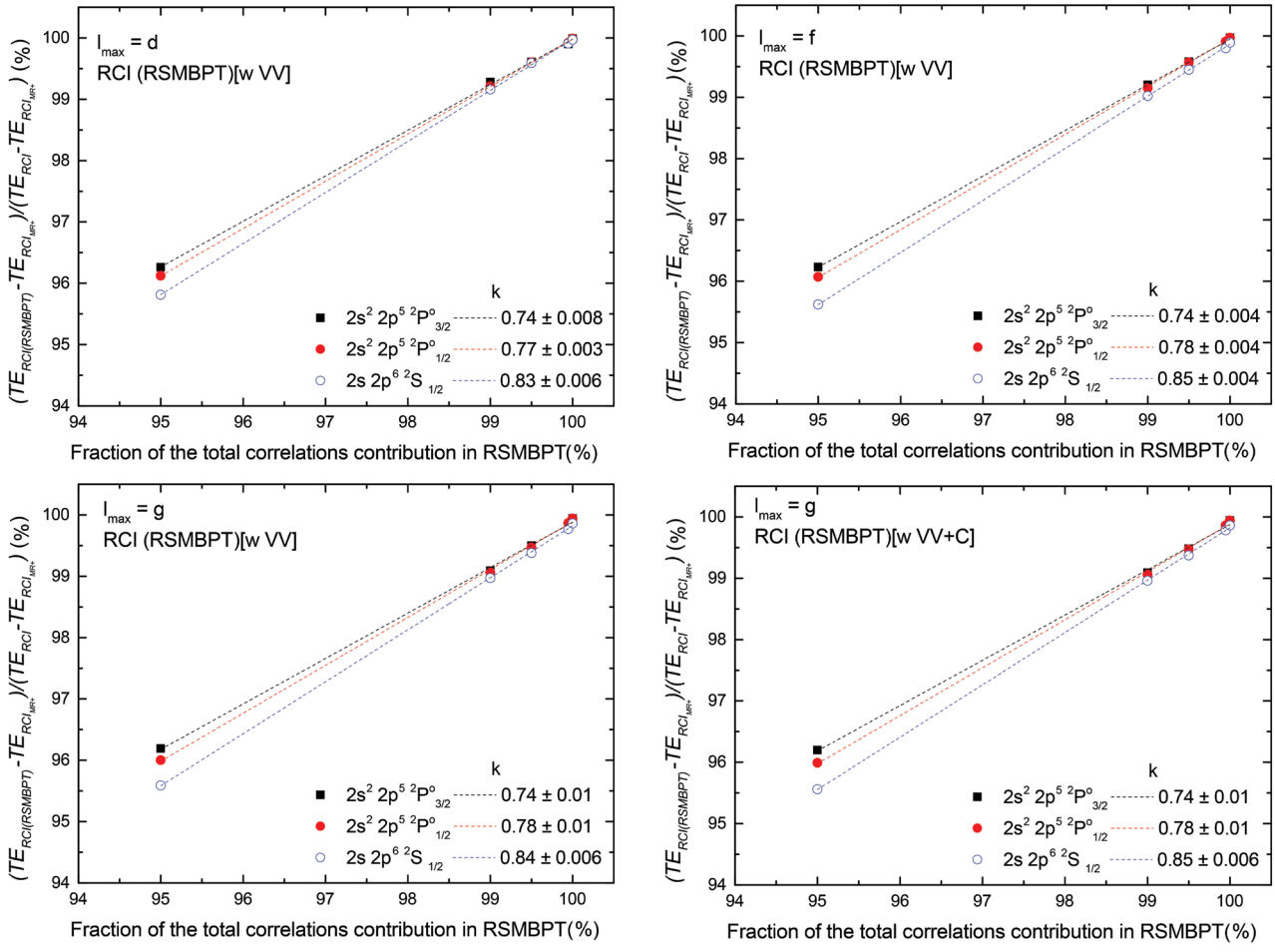

Fig. 6. Dependence of the included correlation contribution (CV+C+CC+VV) on the specified fraction of the total correlation contribution used in the RCI (RSMBPT) method for the three lowest levels, for l_{max} = d, f, g, and for the radial wave functions computed with the VV+C correlations.

on these observations, it can be concluded that the difference between the correlation value (in %) in the predefined RSMBPT calculations and 100% indicates the percentage error in the total energy, which is defined as the difference between the total energy calculated using the regular RCI method (or using the 100% correlations in the RSMBPT method) and the total energy calculated using the reduced correlation obtained due to the shortening of the CSF base. For example, using the RSMBPT method total energies can be analyzed from reduced CSF bases (e.g. 95 and 99% correlation inclusion), and it is possible to accurately extrapolate the total energy that would be obtained when 100% of the correlations are included. The extrapolation of the total energies would be helpful for complex computations when considering CV, C, CC and VV correlations, as such computations lead to a large CSFs basis and are time consuming. Moreover, these regularities remain stable across different orbital symmetries of the virtual space and for different types of correlations included in the radial wave function calculations.

Moreover, these regularities remain stable across different orbital symmetries of the virtual space and for different types of correlations included in the calculations of radial wave function. It is worth noting that this theory has been developed only recently; therefore, it is important to investigate this dependence in greater detail.

Table 5 gives a summary of CSF numbers (N_{CSFs}) for regular **VV MCDHF** and **VV+C MCDHF** computations at OS_{1-5}, for all tested orbitals' symmetries l_{max} = d, f, g. Also, CSF numbers are given for **RCI[w VV]**, **RCI[w VV+C]**, **RCI (RSMBPT)[w VV]** and **RCI (RSMBPT)[w VV+C]** at OS_5 for all tested orbitals' symmetries. For the RCI (RSMBPT) method, the number of CSF is given, based on the amount: 95, 99, 99.5, 99.95 and 100% of CV, C, CC and VV correlations.

Table 5. Summary of the N_{CSF} of standard **VV MCDHF** at OS_1–OS_5 and **RCI[w VV]** methods at OS_5, **RCI (RSMBPT) [w VV]** and **RCI (RSMBPT)[w VV+C]** method at OS_5 is given for l_{max} = {d, f, g}.

OS	l_{max} = d		l_{max} = f		l_{max} = g		l_{max} = g	
	odd	even	odd	even	odd	even	odd	even
	VV MCDHF						**VV+C MCDHF**	
OS_1	54 211	20 344	89 972	35 176	89 972	35 176	96 489	37 038
OS_2	145 282	57 840	271 771	109 930	345 267	137 263	357 960	140 955
OS_3	280 694	114 796	552 878	226 570	770 998	308 520	789 867	314 042
OS_4	460 447	191 212	933 293	385 096	1 367 165	548 947	1 392 210	556 299
OS_5	684 541	287 088	1 413 016	585 508	2 133 768	858 544	2 164 989	867 726
	RCI [w VV]						**RCI[w VV+C]**	
OS_5	2 289 812	912 457	4 942 682	1 877 232	7 560 326	2 762 366	7 560 326	2 762 366
	RCI (RSMBPT)[w VV]						**RCI (RSMBPT)[w VV+C]**	
100%	2 021 303	751 965	3 956 501	1 343 439	5 561 569	1 781 337	5 561 318	1 776 353
99.95%	1 854 036	689 899	3 596 224	1 230 114	4 885 122	1 603 363	4 872 057	1 602 918
99.5%	1 541 262	564 815	2 790 520	954 137	3 652 743	1 216 955	3 636 767	1 214 179
99%	1 375 125	508 995	2 431 184	821 764	3 068 926	1 018 785	3 045 360	1 009 776
95%	851 113	295 434	1 166 070	420 313	1 360 698	484 347	1 347 035	487 039

As seen from the Table 5, even counting the simplest type of correlations, i.e. VV electron correlations with increasing *OS*, N_{CSFs} grows very fast, even without including very high orbital symmetries, such as h or higher (see N_{CSFs} at **VV MCDHF** at OS_5 with orbital symmetries up to g). The inclusion of CV, C and CC correlations of the 1s orbital increases the size of the bases by a factor of 3.2–4.3 (see the data of **RCI [w VV]** and **RCI [w VV+C]** methods). Meanwhile, the RCI (RSMBPT) method reduces N_{CSFs} by 12–36%, even in the case when 100% of correlations are included and this reduction is more prominent at larger *l* symmetries. This reduction is crucial for performing highly accurate calculations, which often require large orbital *l* symmetries and consequently lead to very large CSF bases.

5.2.2. Quantitative and qualitative evaluation

The transition properties of 32 E1-type transitions between the levels of even configurations with J = 1/2 and the levels of odd configurations with J = 1/2 and 3/2 were computed. The calculations are done in a regular way and using the RSMBPT method when CV, C, CC and VV are included. The quantitative and qualitative evaluation method (QQE) [24–26] has been used to investigate the uncertainty of the line strengths (S). Within the QQE method, the minimum of the parabola $G_{S=0}$ [24] values were determined for each transition and subsequently used to assign the corresponding accuracy classes. The accuracy classes match the NIST ASD [23] terminology (AA ≤ 1 %, A+ ≤ 2 %, A ≤ 3 %, B+ ≤ 7 %, B ≤ 10 %, C+ ≤ 18 %, C ≤ 25 %, D+ ≤ 40 %, D ≤50 %, and E > 50 %). The $G_{S=0}$ values for each line strength computed using the standard **RCI [w VV]** method and the **RCI (RSMBPT) [w VV]** method with 100% of the correlations included are shown in Fig. 7 for l_{max} = d, f, g. The Figure also includes the results obtained using radial wave functions that incorporate both C and VV correlations, namely the **RCI [w VV+C]** and **RCI (RSMBPT)[w VV+C]** schemes with 100% of the correlations included. These correlations were included up to the virtual orbital sets OS_5.

As can be seen from Fig. 7, the majority of *S* values calculated using the RCI (RSMBPT) method with 100% of the correlations included coincide with those obtained using the standard RCI method in most cases, independently of the orbital symmetry and of the correlations included in the calculation of the radial wave functions. Noticeable differences are observed only for the smallest *S* values.

Figure 7 also shows that when using the RCI (RSMBPT) method with 100% correlations, in most cases, $G_{S=0}$ values are obtained that correspond to those obtained using the standard RCI method. Small differences are observed for

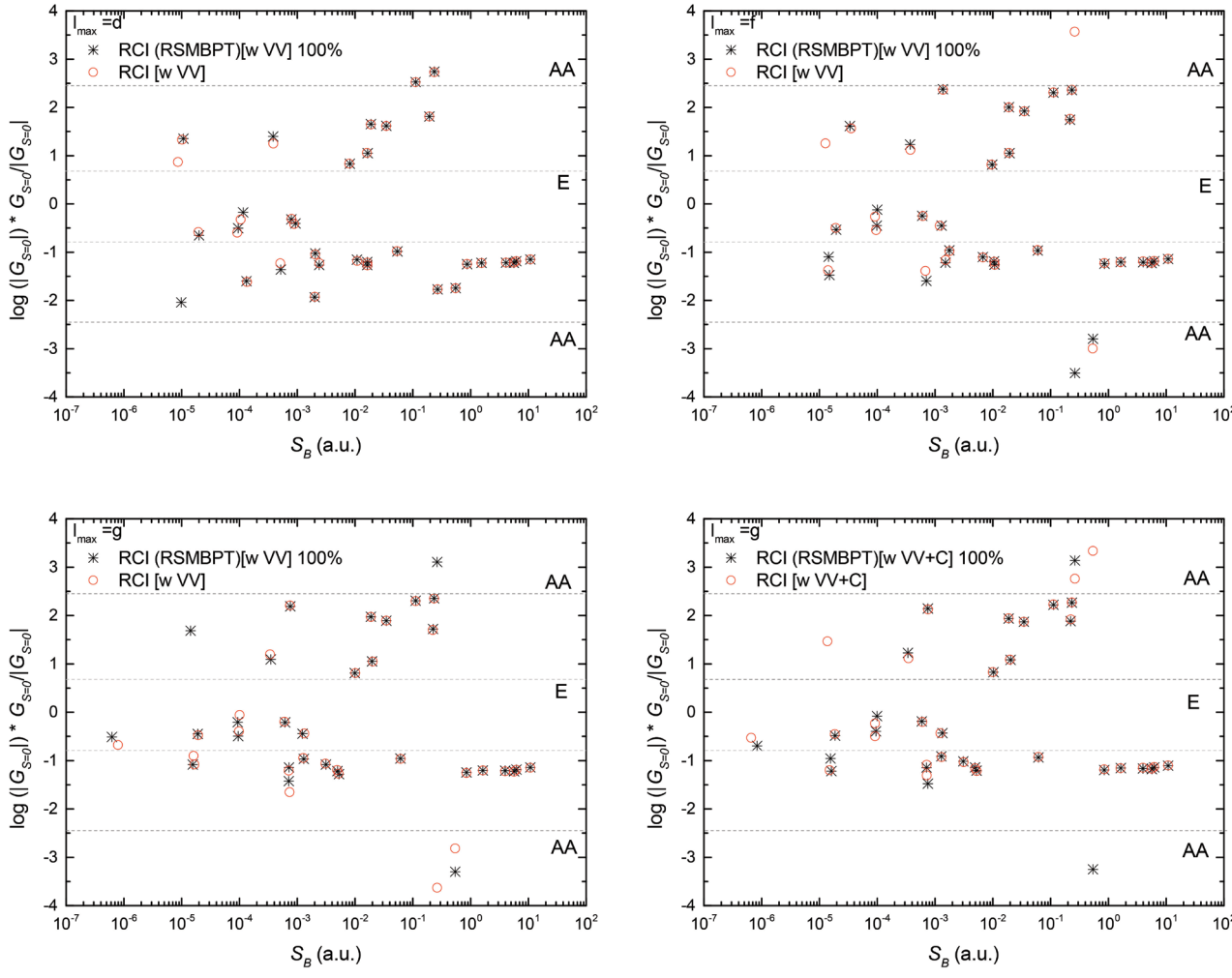

Fig. 7. The $G_{S=0}$ values for each line strength computed using the standard **RCI [w VV]** method and the **RCI (RSMBPT) [w VV]** method with 100% of the correlations included for l_{max} = d, f, g and the **RCI [w VV+C]** and **RCI (RSMBPT) [w VV+C]** schemes with 100% of the correlations included.

the smallest S values, while larger deviations appear for the largest $G_{S=0}$ values, which correspond to the highest accuracy classes. In these cases, the sign of the $G_{S=0}$ value changes; however, the accuracy class remains unchanged.

Table 6 presents the line strengths (in the Babushkin gauge) for two transitions, $2s2p^6\ {}^2S_{1/2} \rightarrow 2s^22p^5\ {}^2P^o_{3/2}$ (3–1) and $2s2p^6\ {}^2S_{1/2} \rightarrow 2s^22p^5\ {}^2P^o_{1/2}$ (3–2), which contribute to the lifetime under consideration. The line strengths were calculated using the standard **RCI [w VV]** and **RCI (RSMBPT) [w VV]** methods including virtual orbitals up to OS_5 for l_{max} = d, f, g. Additionally, the results obtained with radial functions that include C and VV correlations are reported for the **RCI [w VV+C]** and **RCI (RSMBPT) [w VV+C]** schemes. The corresponding accuracy classes are also provided. The line strengths calculated using the RCI method coincide with those obtained using the RCI (RSMBPT) method when 100% correlation is included, with differences at the 0.0–0.1% level, independently of the orbital symmetry and the correlations included in the radial function calculations. As the amount of included correlation decreases, the agreement with the standard RCI results slightly deteriorates; however, the relative differences $(S_{RCI} - S_{RCI(RSMBPT_{95\%})})/S_{RCI}$, remain below 0.5%. The accuracy classes of these line strengths, computed using the RCI method, coincide with those obtained using the RCI (RSMBPT) approach when 100% correlation is included, independently of the orbital symmetry and the correlations included in the radial function calculations. As the percentage of included correlation decreases, the accuracy slowly deteriorates.

Table 6. Line strengths (in a.u.) in Babushkin gauge (S_B) for two transitions: $2s2p^6\ ^2S_{1/2} - 2s^22p^5\ ^2P^o_{3/2}$ (3–1) and $2s2p^6\ ^2S_{1/2} - 2s^22p^5\ ^2P^o_{1/2}$ (3–2) computed using standard **VV MCDHF**, **VV+C MCDHF**, **RCI [w VV]** and **RCI[w VV+C]** methods, and **RCI (RSMBPT)[w VV]** and **RCI (RSMBPT)[w VV+C]** methods.

OS	S_B															
	l_{max} = d				l_{max} = f				l_{max} = g				l_{max} = g			
	3–1		3–2		3–1		3–2		3–1		3–2		3–1		3–2	
	VV MCDHF												**VV+C MCDHF**			
OS_1	3.439E-01	AA	1.537E-01	AA	5.156E-01	A+	2.393E-01	A+	5.156E-01	A+	2.393E-01	A+	6.192E-01	A	2.931E-01	A
OS_2	5.412E-01	A	2.658E-01	A	5.471E-01	A+	2.688E-01	A	5.568E-01	A+	2.729E-01	A	5.356E-01	A	2.647E-01	A
OS_3	5.406E-01	A	2.648E-01	A	5.419E-01	A+	2.649E-01	A	5.489E-01	A+	2.680E-01	A	5.411E-01	A	2.651E-01	A
OS_4	5.387E-01	A	2.623E-01	A	5.308E-01	A+	2.578E-01	A	5.362E-01	A+	2.605E-01	A	5.317E-01	A	2.584E-01	A
OS_5	5.385E-01	A	2.623E-01	A	5.307E-01	A+	2.579E-01	A	5.363E-01	A+	2.606E-01	A+	5.315E-01	A	2.584E-01	A
	RCI [w VV]												**RCI[w VV+C]**			
OS_5	5.496E-01	B+	2.680E-01	B+	5.384E-01	AA	2.625E-01	AA	5.414E-01	AA	2.645E-01	AA	5.415E-01	AA	2.645E-01	AA
	RCI (RSMBPT)[w VV]												**RCI (RSMBPT)[w VV+C]**			
100%	5.498E-01	B+	2.681E-01	B+	5.387E-01	AA	2.627E-01	AA	5.418E-01	AA	2.647E-01	AA	5.419E-01	AA	2.647E-01	AA
99.95%	5.503E-01	B+	2.681E-01	B+	5.393E-01	AA	2.627E-01	AA	5.424E-01	AA	2.647E-01	AA	5.425E-01	AA	2.647E-01	AA
99.5%	5.506E-01	B+	2.684E-01	B+	5.397E-01	AA	2.629E-01	AA	5.429E-01	AA	2.648E-01	AA	5.431E-01	AA	2.648E-01	AA
99%	5.507E-01	B+	2.684E-01	B+	5.404E-01	A+	2.633E-01	AA	5.433E-01	AA	2.652E-01	AA	5.434E-01	AA	2.653E-01	AA
95%	5.495E-01	B+	2.684E-01	B+	5.399E-01	A	2.631E-01	A+	5.436E-01	A	2.654E-01	A+	5.440E-01	A	2.654E-01	AA

5.2.3. Lifetime

Table 7 presents the lifetime of the $2s2p^6\ ^2S_{1/2}$ state. The lifetime was calculated using the standard MCDHF method, which includes only VV correlations in different virtual orbital sets (OS_1 through OS_5), restricted by orbital symmetry (l_{max} = d, f, g). The Table also presents the results obtained using the RCI and RCI (RSMBPT) methods with the virtual orbital setup to OS_5, under the same

Table 7. Lifetime (in ns) of the $2s2p^6\ ^2S_{1/2}$ state is computed using the standard **VV MCDHF**, **VV+C MCDHF** and **RCI [w VV]** and **RCI [w VV+C]** methods, and the **RCI (RSMBPT)[w VV]** and **RCI (RSMBPT)[w VV+C]** methods. Lifetimes are given in the Babushkin and Coulomb (in parentheses) gauges.

OS	τ			
	l_{max} = d	l_{max} = f	l_{max} = g	l_{max} = g
	VV MCDHF			**VV+C MCDHF**
MR	0.1171 (0.09761)	0.1171 (0.09761)	0.1171 (0.09761)	0.1171 (0.09761)
OS_1	0.1991 (0.2007)	0.1991 (0.2007)	0.1287 (0.1262)	0.1066 (0.1042)
OS_2	0.1223 (0.1258)	0.1187 (0.1165)	0.1165 (0.1140)	0.1207 (0.1180)
OS_3	0.1223 (0.1259)	0.1198 (0.1175)	0.1182 (0.1156)	0.1196 (0.1169)
OS_4	0.1229 (0.1265)	0.1227 (0.1202)	0.1213 (0.1186)	0.1222 (0.1195)
OS_5	0.1229 (0.1264)	0.1227 (0.1202)	0.1212 (0.1185)	0.1222 (0.1195)
	RCI [w VV]			**RCI [w VV+C]**
OS_5	0.1231 (0.1293)	0.1236 (0.1238)	0.1226 (0.1227)	0.1231 (0.1228)
	RCI (RSMBPT)[w VV]			**RCI (RSMBPT)[w VV+C]**
100%	0.1231 (0.1293)	0.1235 (0.1239)	0.1225 (0.1229)	0.1230 (0.1231)
99.95%	0.1230 (0.1297)	0.1234 (0.1242)	0.1224 (0.1233)	0.1229 (0.1234)
99.5%	0.1230 (0.1300)	0.1233 (0.1244)	0.1224 (0.1234)	0.1228 (0.1235)
99%	0.1230 (0.1302)	0.1232 (0.1244)	0.1223 (0.1234)	0.1228 (0.1235)
95%	0.1233 (0.1321)	0.1235 (0.1239)	0.1224 (0.1249)	0.1228 (0.1250)
Ex. [27]	0.132			
Th. [27]	0.120 (0.126)			
Th. [28]	0.1214			

orbital-symmetry constraints as in the MCDHF calculations. Various percentages of CV, C, CC and VV correlations (95, 99, 99.5, 99.95 and 100%) were included in the RCI (RSMBPT) calculations. Lifetimes are reported in the Babushkin gauge, with values in the Coulomb gauge given in brackets.

The lifetime in the Babushkin gauge of the $2s2p^6\ ^2S_{1/2}$ state is reproduced, using the RCI (RSMBPT) method in the case of the '100%', with a precision of 4 digits (i.e. $\tau_{\mathrm{RCI(RSMBPT)}} - \tau_{\mathrm{RCI}} = 0.0001$) compared to the regular Grasp2018 calculations, irrespective of the orbital symmetries that are included in the calculations and of the types of correlations included in radial function computations. The lifetime in Coulomb's gauge is reproduced with a precision of 4 digits (i.e. $\tau_{\mathrm{RCI(RSMBPT)}} - \tau_{\mathrm{RCI}} \leq 0.0003$).

The lifetime is also very stable with decreasing correlation percentage regardless of the orbital symmetry included. The difference in lifetimes between the 100 and 95% cases is also small ($\tau_{\mathrm{RCI(RSMBPT_{100\%})}} - \tau_{\mathrm{RCI(RSMBPT_{95\%})}} \leq 0.0002$ for Babushkin's gauge and ≤ 0.0028 for Coulomb's gauge).

The experimental [27] and theoretical [27, 28] lifetimes are given for comparison. Experiment was done using the time-correlated single photon counting technique combined with photoionization by synchrotron radiation. Theoretical computations for lifetime are done using the multi-configuration Dirac–Fock method in the same work [27]. The lifetimes from the last investigation are given in the Babushkin and in the Coulomb (in parentheses) gauges. The next theoretical work [28] was done using the multi-configuration Hartree–Fock method with the relativistic effects included through the Breit–Pauli Hamiltonian, omitting only the orbit–orbit interaction.

Our calculated lifetime using the RCI (RSMBPT) and regular RCI methods is smaller than the experimentally measured value [27], but slightly bigger than the theoretical evaluation by Refs. [27] and [28].

6. Conclusions

The method, based on the Rayleigh–Schrödinger perturbation theory in an irreducible tensorial form, is extended to estimate the CV correlations of the third and fourth types. We provided the analytical expression of a three-particle Feynman diagram describing these CV correlations with explanations and expression for the spin-angular coefficients. The expressions to calculate the influence of these correlations are derived and provided. This extended RSMBPT method allows us to evaluate the contribution of each K' configuration, which determines one of the CV, C, CC, or VV correlation types, to the CSFs in the MR set. The method applies to the investigation of correlations in arbitrary electronic configurations of atoms or ions, using selected core and virtual orbital sets and allowing for any number of valence electrons. The 12 lowest energy levels of the $2s^22p^5$, $2s2p^6$ and $2s^22p^4\{3s, 3p\}$ configurations, the properties of 32 E1-type transitions between those levels, and the lifetime of $2s2p^6\ ^2S_{1/2}$ state were computed for Ne II.

The analysis of the energy levels has shown that the RCI (RSMBPT) method reproduces the regular RCI energy levels independently of the orbital symmetry of the virtual orbitals. In addition, the ability of the RCI (RSMBPT) method to reproduce the energy levels is independent of the type of correlations included in the regular MCDHF computations.

Using the RSMBPT method total energies can be analyzed from reduced CSF bases (e.g. 95 and 99% correlation inclusion), and it is possible to accurately extrapolate the total energy that would be obtained when 100% of the correlations are included. The extrapolation of the total energies would be helpful for complex computations when considering CV, C, CC and VV correlations, as such computations lead to a large CSFs basis and are time consuming. Moreover, these regularities remain stable across different orbital symmetries of the virtual space and for different types of correlations included in the radial wave function calculations.

The accuracy classes of the line strengths for transitions originating from the $2s2p^6\ ^2S_{1/2}$ state coincide when 100% of correlations were included in the **RCI(RSMBPT) [w VV]** and **RCI(RSMBPT) [w VV+C]** schemes. As the percentage of included correlations decreases, the accuracy classes gradually deteriorate.

The lifetime of the $2s2p^6\ ^2S_{1/2}$ state is reproduced using the RCI(RSMBPT) method with 100% of the correlations included, with a precision of four digits (i.e. $\tau_{\mathrm{RCI(RSMBPT)}} - \tau_{\mathrm{RCI}} = 0.0001$ in the Babushkin gauge and ≤ 0.0003 in the Coulomb gauge), compared to the regular Grasp2018 calculations, independently of the orbital symmetries included in the calculations and of the types of correlations

included in the radial wave-function computations. The lifetime is also very stable with decreasing correlation percentage regardless of the orbital symmetry inclusion. The difference in lifetimes in the cases 100 and 95% is also small ($\tau_{\mathrm{RCI(RSMBPT_{100\%})}} - \tau_{\mathrm{RCI(RSMBPT_{95\%})}} \leq 0.0002$ for Babushkin's gauge and ≤ 0.0028 for Coulomb's gauge). The same stability of the lifetime value is observed when the radial functions are calculated by including the VV+C correlation.

References

[1] I. Lindgren and J. Morrison, *Atomic Many-body Theory* (Springer-Verlag Berlin Heidelberg, New York, 1982).

[2] G. Gaigalas, P. Rynkun, and L. Kitovienė, Second-order Rayleigh–Schrödinger perturbation theory for the Grasp2018 package: Core–valence correlations, Lith. J. Phys. **64**(1), 20–39 (2024), https://doi.org/10.3952/physics.2024.64.1.3

[3] G. Gaigalas, P. Rynkun, and L. Kitovienė, Second-order Rayleigh–Schrödinger perturbation theory for the Grasp2018 package: Core correlations, Lith. J. Phys. **64**(2), 73–81 (2024), https://doi.org/10.3952/physics.2024.64.2.1

[4] G. Gaigalas, P. Rynkun, and L. Kitovienė, Second-order Rayleigh–Schrödinger perturbation theory for the Grasp2018 package: Core–core correlations, Lith. J. Phys. **64**(3), 139–161 (2024), https://doi.org/10.3952/physics.2024.64.3.1

[5] G. Gaigalas, P. Rynkun, and L. Kitovienė, Second-order Rayleigh–Schrödinger perturbation theory for the Grasp2018 package: Valence–valence correlations, Lith. J. Phys. **65**(1), 32–56 (2025), https://doi.org/10.3952/physics.2025.65.1.2

[6] G. Gaigalas, P. Rynkun, and L. Kitovienė, Second-order Rayleigh–Schrödinger perturbation theory for the Grasp2018 package: Three-particle Feynman diagram contribution to valence–valence correlations, Lith. J. Phys. **65**(2), 81–106 (2025), https://doi.org/10.3952/physics.2025.65.2.2

[7] C. Froese Fischer, G. Gaigalas, P. Jönsson, and J. Bieroń, Grasp2018 – A Fortran 95 version of the General Relativistic Atomic Structure Package, Comput. Phys. Commun. **237**, 184–187 (2019), https://doi.org/10.1016/j.cpc.2018.10.032

[8] R. Si, Y. Li, K. Wang, Ch. Chen, G. Gaigalas, M. Godefroid, and P. Jönsson, GraspG – An extension to Grasp2018 based on configuration state function generators, Comput. Phys. Commun. **312**, 109604 (2025), https://doi.org/10.1016/j.cpc.2025.109604

[9] I.P. Grant, *Relativistic Quantum Theory of Atoms and Molecules* (Springer, New York, 2007).

[10] C. Froese Fischer, M. Godefroid, T. Brage, P. Jönsson, and G. Gaigalas, Advanced multiconfiguration methods for complex atoms: I. Energies and wave functions, J. Phys. B **49**(18), 182004 (2016), https://doi.org/10.1088/0953-4075/49/18/182004

[11] P. Jönsson, M. Godefroid, G. Gaigalas, J. Ekman, J. Grumer, W. Li, J. Li, T. Brage, I.P. Grant, J. Bieroń, and C. Froese Fischer, An introduction to relativistic theory as implemented in Grasp, Atoms **11**, 7 (2023), https://doi.org/10.3390/atoms11010007

[12] P. Jönsson, G. Gaigalas, Ch. F. Fischer, J. Bieroń, I.P. Grant, T. Brage, J. Ekman, M. Godefroid, J. Grumer, J. Li, and W. Li, Grasp Manual for Users, Atoms **11**, 68 (2023), https://doi.org/10.3390/atoms11040068

[13] G. Gaigalas, Z. Rudzikas, and C. Froese Fischer, An efficient approach for spin-angular integrations in atomic structure calculations, J. Phys. B **30**(17), 3747 (1997), https://doi.org/10.1088/0953-4075/30/17/006

[14] G. Gaigalas, Extension of an efficient approach for spin-angular integrations in atomic structure calculations, Atoms **14**(21), 1–28 (2026), https://doi.org/10.3390/atoms14030021

[15] G. Gaigalas, A program library for computing pure spin-angular coefficients for one- and two-particle operators in relativistic atomic theory, Atoms **10**(4), 129 (2022), https://doi.org/10.3390/atoms10040129

[16] G. Gaigalas and Z. Rudzikas, On the secondly quantized theory of the many-electron atom, J. Phys. B **29**(15), 3303 (1996), https://doi.org/10.1088/0953-4075/29/15/007

[17] G. Gaigalas, Diagrammatic approach to irreducible tensorial operators and its application to perturbation theory, in: *Spectroscopy of Autoionized States of Atoms and Ions* (Scientific

Council of Spectroscopy, Moscow, 1985) pp. 43–61 [in Russian].

[18] G. Gaigalas, *Irreducible Tensorial Form of the Stationary Perturbation Theory for Atoms and Ions with Open Shells*, PhD Thesis (Institute of Physics, Vilnius, 1989), https://kolekcijos.biblioteka.vu.lt/en/objects/990007058341008452#00001 [in Russian].

[19] B.R. Judd, *Second Quantization and Atomic Spectroscopy* (The Johns Hopkins Press, Baltimore, 1967).

[20] G. Gaigalas, J.G. Kaniauskas, and Z. Rudzikas, Diagrammatic technique of the angular momentum theory and second quantization, Liet. Fiz. Rink. (Sov. Phys. Coll.) **25**, 3–13 (1985) [in Russian].

[21] A.P. Jucys and A.A. Bandzaitis, *Theory of Angular Momentum in Quantum Mechanics* (Mokslas, Vilnius, 1977) [in Russian].

[22] Y.T. Li, K. Wang, R. Si, M. Godefroid, G. Gaigalas, Ch.Y. Chen, and P. Jönsson, Reducing the computational load – atomic multiconfiguration calculations based on configuration state function generators, Comput. Phys. Commun. **283**, 108562 (2023), https://doi.org/10.1016/j.cpc.2022.108562

[23] A. Kramida, Yu. Ralchenko, J. Reader, and NIST ASD Team, *NIST Atomic Spectra Database*, Version 5.12 (National Institute of Standards and Technology, Gaithersburg, MD, 2024), https://physics.nist.gov/asd

[24] L. Kitovienė, G. Gaigalas, P. Rynkun, M. Tanaka, and D. Kato, Theoretical investigation of the Ge isoelectronic sequence, J. Phys. Chem. Ref. Data **53**, 033101 (2024), https://doi.org/10.1063/5.0187307

[25] P. Rynkun, S. Banerjee, G. Gaigalas, M. Tanaka, L. Radžiūtė, and D. Kato, Theoretical investigation of energy levels and transition for Ce IV, A&A **658**, A82 (2022), https://doi.org/10.1051/0004-6361/202141513

[26] G. Gaigalas, P. Rynkun, S. Banerjee, M. Tanaka, D. Kato, and L. Radžiūtė, Theoretical investigation of energy levels and transition for Pr IV, MNRAS **517**, 281 (2022), https://doi.org/10.1093/mnras/stac2401

[27] N. Suzuki, S. Kosugi, Y. Ito, N. Inoue, T. Nagoshi, N. Kuze, J.R. Harries, J.P. Sullivan, T. Nagata, E. Sokell, F. Koike, and Y. Azuma, Probing electron correlation through radiative lifetime measurements upon inner-valence photoionization of Ne and Ar, J. Phys. B **49**, 145002 (2016), https://doi.org/10.1088/0953-4075/49/14/145002

[28] C.F. Fischer and G. Tachiev, Breit–Pauli energy levels, lifetimes, and transition probabilities for the beryllium-like to neon-like sequences, At. Data Nucl. Data Tables **87**, 1–184 (2004), https://doi.org/10.1016/j.adt.2004.02.001

ANTROSIOS EILĖS RELĖJAUS IR ŠRĖDINGERIO TRIKDYMŲ TEORIJA GRASP2018 PROGRAMINIAM PAKETUI: TRIJŲ DALELIŲ FEINMANO DIAGRAMOS ĮTAKA KAMIENO–VALENTINĖMS KORELIACIJOMS

G. Gaigalas, P. Rynkun, L. Kitovienė

Vilniaus universiteto Fizikos fakulteto Teorinės fizikos ir astronomijos institutas, Vilnius, Lietuva

Santrauka

Išplėtotas antrosios eilės trikdymų teorija paremtas metodas, skirtas įvairių koreliacijų vertei nustatyti, įtraukiant kamieno–valentines koreliacijas, kurios aprašomos trijų dalelių Feinmano diagrama. Darbe pateiktas išplėtimas papildo kamieno–valentines, kamieno, kamieno–kamieno ir valentines–valentines koreliacijas, kurios buvo išplėtotos ankstesniuose G. Gaigalo, P. Rynkun ir L. Kitovienės darbuose, trečio ir ketvirto tipo kamieno–valentinėmis koreliacijomis. Kadangi šios koreliacijos aprašomos trijų dalelių Feinmano diagrama, papildomai buvo atlikti pakeitimai ir išplėtimai GRASP programos bibliotekoje „`librang`“, siekiant apskaičiuoti šios diagramos sukinines-kampines dalis. Remiantis pateiktuoju išplėtimu, buvo atrinktos svarbiausios konfigūracinių būsenų funkcijos reliatyvistiniui konfigūracijų superpozicijos metodui. Darbe, kaip metodo taikymo pavyzdys, taip pat pateikiami Ne II energijos struktūros, šuolių parametrų ir gyvavimo trukmės skaičiavimai.